iScience

CellPress

Article

ORCA/LRWD1 Regulates Homologous Recombination at ALT-Telomeres by Modulating Heterochromatin Organization

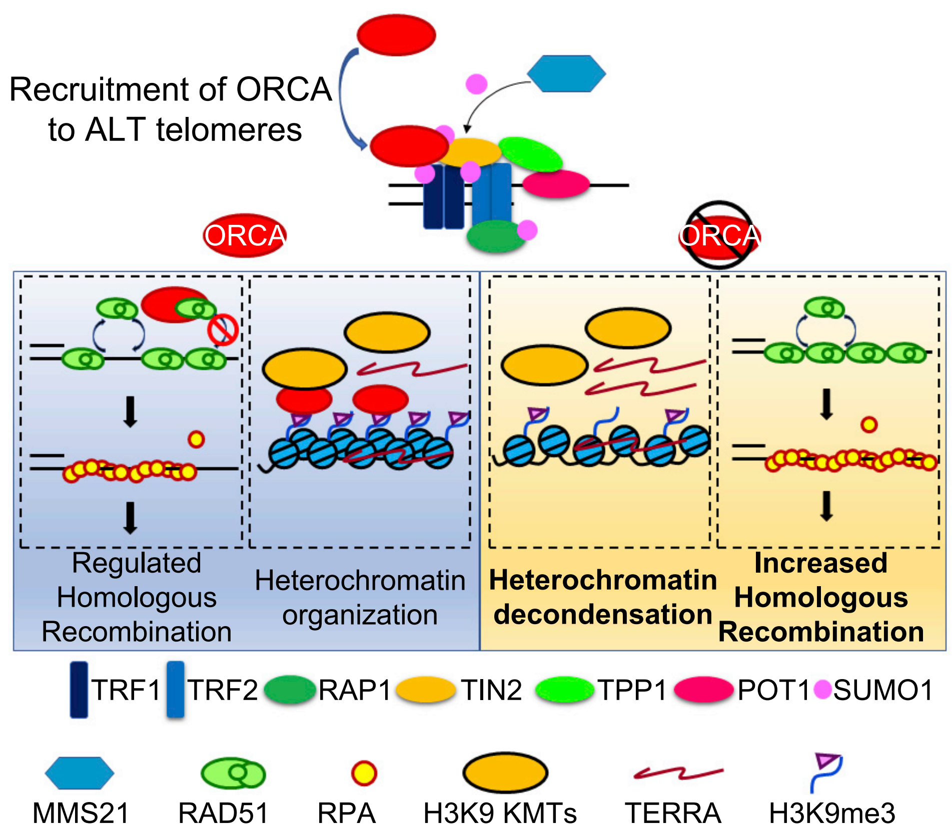

Rosaline Y.C. Hsu, Yo-Chuen Lin, Christophe Redon, ..., Mirit I. Aladjem, Kannanganattu V. Prasanth, Supriya G. Prasanth

supriyap@illinois.edu

HIGHLIGHTS

ORCA is enriched at ALT-telomeres

The SUMOylation of shelterin components is essential for ORCA recruitment to telomeres

ORCA negatively regulates ALT activity

ORCA regulates HR by modulating heterochromatin compaction and RPA binding to ssDNA

DATA AND CODE AVAILABILITY

GSE81165

Hsu et al., iScience 23, 101038
May 22, 2020
https://doi.org/10.1016/j.isci.2020.101038

iScience

CellPress

Article

ORCA/LRWD1 Regulates Homologous Recombination at ALT-Telomeres by Modulating Heterochromatin Organization

Rosaline Y.C. Hsu,[1] Yo-Chuen Lin,[1] Christophe Redon,[2] Qinyu Sun,[1] Deepak K. Singh,[1] Yating Wang,[1] Vasudha Aggarwal,[3] Jaba Mitra,[4] Abhijith Matur,[1] Branden Moriarity,[5] Taekjip Ha,[3,6] Mirit I. Aladjem,[2] Kannanganattu V. Prasanth,[1,7] and Supriya G. Prasanth[1,7,*]

SUMMARY

Telomeres are maintained by telomerase or in a subset of cancer cells by a homologous recombination (HR)-based mechanism, Alternative Lengthening of Telomeres (ALT). The mechanisms regulating telomere-homeostasis in ALT cells remain unclear. We report that a replication initiator protein, Origin Recognition Complex-Associated (ORCA/LRWD1), by localizing at the ALT-telomeres, modulates HR activity. ORCA's localization to the ALT-telomeres is facilitated by its interaction to SUMOylated shelterin components. The loss of ORCA in ALT-positive cells elevates the levels of two mediators of HR, RPA and RAD51, and consistent with this, we observe increased ALT-associated promyelocytic leukemia body formation and telomere sister chromatid exchange. ORCA binds to RPA and modulates the association of RPA to telomeres. Finally, the loss of ORCA causes global chromatin decondensation, including at the telomeres. Our results demonstrate that ORCA acts as an inhibitor of HR by modulating RPA binding to ssDNA and inducing chromatin compaction.

INTRODUCTION

Accurate duplication of the genetic material and the faithful segregation of the chromosomes to the daughter nuclei are paramount to cell survival. The integrity of the genome requires efficient and regulated mechanisms that control chromatin replication, telomere maintenance, centrosome numbers, and centromere integrity. In mammalian cells, Origin Recognition Complex (ORC) regulates DNA replication initiation, chromatin organization, and chromosome segregation (Blow and Tanaka, 2005; Stillman, 2005). In addition, ORC is involved in many other cellular processes, including gene silencing, centrosome duplication, heterochromatin organization, and cytokinesis (Bell and Dutta, 2002; Bell and Stillman, 1992; Prasanth et al., 2002, 2004, 2010; Sasaki and Gilbert, 2007).

Several years ago, we identified a highly conserved, leucine-rich repeat and WD repeat-containing protein (LRWD1), or ORC-Associated (ORCA), in human cells that interacts with ORC. ORCA modulates the chromatin association of ORC and is required for DNA replication initiation (Shen et al., 2010, 2012). ORCA and ORC associate with specialized heterochromatic structures, including centromeres and telomeres and regulate heterochromatin organization (Craig et al., 2003; Giri and Prasanth, 2015; Ohta et al., 2010; Prasanth et al., 2002, 2004, 2010; Shen et al., 2010). ORCA binds to repressive histone marks, including H3K9me3, H4K20me3, and H3K27me3 and associates with the machinery that establishes repressive modifications (Bartke et al., 2010; Giri et al., 2015; Shen et al., 2010; Vermeulen et al., 2010). Our results point to a model that ORCA acts as a scaffold protein that enables the association of multiple histone lysine methyltransferase and DNA methyltransferase complexes at the heterochromatic sites, thereby facilitating heterochromatin organization. We have previously demonstrated that the role of ORCA in heterochromatin organization is independent of its role in DNA replication initiation (Giri et al., 2015). However, the functional relevance of ORC/ORCA binding to telomeres and to centromeres remains to be identified.

Telomeres are specialized heterochromatic structures at the ends of eukaryotic linear chromosomes. The mammalian telomeres consist of TTAGGG repetitive DNA that is associated with the shelterin, a six-protein complex (TRF1, TRF2, hRAP1, POT1, TIN2, TPP1), which is critical for telomere maintenance and genome stability. Telomeres represent constitutive heterochromatin and are enriched for H3K9me3 and HP1 proteins (Blasco, 2007). Also, in most eukaryotes, telomeres transcribe a heterogeneous long

[1]Department of Cell and Developmental Biology, University of Illinois at Urbana-Champaign, 601S Goodwin Avenue, Urbana, IL 61801, USA

[2]Developmental Therapeutics Branch, Center for Cancer Research, NCI, NIH, Bethesda MD 20892, USA

[3]Biophysics and Biophysical Chemistry, Johns Hopkins University, Baltimore, MD 21205, USA

[4]Materials Engineering Department, UIUC, Urbana, IL 61801, USA

[5]Department of Pediatrics, University of Minnesota, MN 55455 USA

[6]Howard Hughes Medical Institute, Johns Hopkins University, Baltimore, MD 21205, USA

[7]Cancer Center at Illinois, UIUC, Urbana, IL 61801, USA

*Correspondence: supriyap@illinois.edu

https://doi.org/10.1016/j.isci.2020.101038

non-coding RNA, TERRA (telomeric repeat-containing RNA) (Azzalin et al., 2007; Schoeftner and Blasco, 2008), that contributes to telomeric heterochromatin formation by promoting H3K9 trimethylation (Arnoult et al., 2012; Deng et al., 2009). Telomeres are maintained either by telomerase, a specialized reverse transcriptase, which utilizes an RNA template to elongate the telomeric sequences, or by a recombination-based mechanism, called the Alternative Lengthening of Telomeres (ALT) (Murnane et al., 1994; Victoria Lundblad, 1993). ALT is utilized by 10%–15% cancer cells from mostly mesenchymal origin. The hallmarks of ALT cells include heterogeneous telomere lengths (Bryan et al., 1995), high levels of telomere sister chromatid exchanges (T-SCEs) (Londoño-Vallejo et al., 2004), ALT-associated promyelocytic leukemia (PML) bodies (APBs) (Yeager et al., 1999), and extrachromosomal telomeric repeat DNA (Cesare and Griffith, 2004). Why certain tumors activate the ALT pathway remains to be understood (Dilley and Greenberg, 2015).

Others and we have observed that ORC and ORCA associate with telomeres. ORC has been found to localize to telomere repeats and prevent telomere circle formation (Deng et al., 2007). Loss of Orc1 was also found to increase telomere length, suggesting that ORC might be involved in telomere homeostasis in human cells (Tatsumi et al., 2008). We previously reported that ORC and ORCA associate predominantly with telomeres of cells that utilize ALT (Shen et al., 2010). However, the functional relevance of this association, and why ORC/ORCA are enriched at telomeres of ALT-positive cells relative to telomerase-positive cells, is unknown.

In the current study, we demonstrate that ORCA binds to ALT-telomeres by enhanced interaction with ALT-telomere-specific SUMOylated shelterin components. The loss of ORCA results in elevated levels of RAD51 and RPA at ALT-telomeres and increased formation of APBs and shows elevated level of T-SCEs. Furthermore, cells lacking ORCA show increased frequency of global sister chromatid exchange and chromatin decondensation. Our results point to an important role of ORCA in modulating homologous recombination (HR) level through regulating RPA binding to ssDNA and organizing heterochromatin.

RESULTS

SUMOylation of the Shelterin Complex Is Essential for ORCA Recruitment to ALT-Telomeres

We have previously reported that ORCA is enriched at telomeres of cells that utilize ALT (e.g., U2OS) but not in telomerase-positive cells (e.g., MCF7, HeLa) (Shen et al., 2010). We demonstrate that ORCA as well as Orc1 is enriched at ALT-telomeres (U2OS, SaOS2, and WI38-VA13, Figures 1A, 1B, S1A, S1D, and S1E). The binding of ORCA to telomeres was corroborated using chromatin immunoprecipitation in HA-ORCA-expressing cells (Figures S1B and S1C).

We observed that the extent of ORCA association to telomeres showed excellent correlation with that of Telomeric Repeat binding Factor 2 (TRF2) enrichment at telomeres (Figures S1F and S1G). The level of shelterin components is predicted to be proportional to the telomere length (Loayza and De Lange, 2003). One of the key differences between telomerase-positive cells and ALT-positive cells is the length of telomeres. The average telomere length in telomerase-positive cells is usually less than 10 kb, whereas the average ALT-telomere length is larger than 20 kb (Bryan et al., 1995). One possibility for the enrichment of ORCA at ALT-telomeres (Figure 1A) could be because ALT-telomeres are very long. To investigate if ORCA accumulation correlates to telomere length, we performed ORCA immunofluorescence studies in a telomerase-positive cell line with long telomeres, HeLa 1.2.11 (telomere length $\sim$23 kb) (Takai et al., 2010). ORCA showed limited localization at telomeres in HeLa 1.2.11 cells (Figure 1A, bottom panel), indicating that ORCA enrichment at ALT-telomeres is independent of the telomere length. To determine the minimum telomere localization domain of ORCA, YFP-tagged ORCA WT and different truncation mutants of ORCA were transiently transfected into U2OS cells and co-stained with TRF2. We observed that the WD domain of ORCA was required for its localization at telomeres (Figures S1H–S1J).

To determine how ORCA is recruited to telomeres, we first examined the interaction of ORCA with shelterin. Immunoprecipitation using ORCA antibody revealed that ORCA interacts with the shelterin complex (Figure S1K). The interaction was also confirmed using Single-Molecule Pull down (SiMPull) assay (Figures S1L–S1N). Consistent with our immunofluorescence staining results, the WD domain was required for the interaction with shelterin components (Figure S1O). To determine if the localization of ORCA to telomeres was shelterin complex dependent, we addressed the association of ORCA to telomeres using ChIP and immunofluorescence approaches. The depletion of shelterin components decreased the

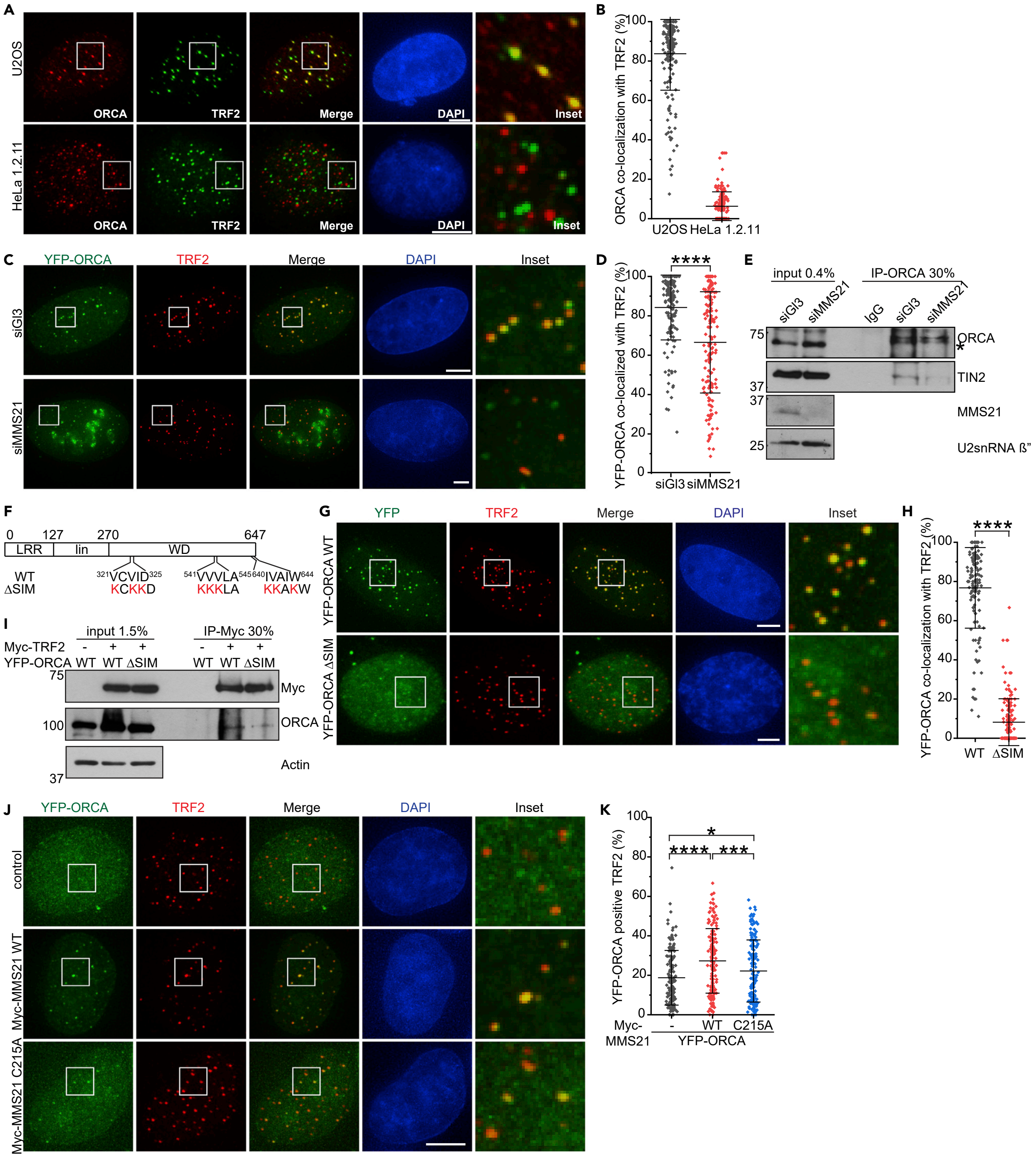

Figure 1. SUMOylation of the Shelterin Complex Is Essential for ORCA Recruitment to ALT-telomeres

(A) Co-immunolocalization of ORCA (red) and telomeres (TRF2, green) in U2OS (ALT) and HeLa 1.2.11 (Telomerase) cells. DNA is stained with DAPI (blue). Scale bar denotes 5 μm. Inset of the merged images is shown.

(B) Quantification of ORCA co-localization with TRF2 per cell. Cell number >160. Values (means ± SD) are from three independent experiments.

(C and D) (C) Representative images of immunofluorescence staining of TRF2 (red) and DNA (DAPI, blue), in U2OS YFP-ORCA stable treated with control or siMMS21. Selected regions of merged images are shown as "Insets." Scale bar denotes 5 μm. (D) The percentage of YFP-ORCA co-localized with TRF2 per cells was measured. Cell number >150. Values (means ± SD) are from three independent experiments. ****, $p < 0.001$.

Figure 1. *Continued*

(E) Immunoprecipitation (IP) of endogenous ORCA in U2OS cells treated with control or siMMS21. The protein complex was analyzed by western blotting. '*' denotes cross-reacting bands.

(F–H) (F) Schematic of ORCA ΔSIM mutant. (G) Representative images of immunofluorescence staining of TRF2 (red) and DNA (DAPI, blue) in U2OS cells transiently expressing YFP-ORCA WT or ΔSIM. Selected region of the merged image is shown as "Inset." Scale bar denotes 5 μm. (H) The percentage of YFP-ORCA co-localized with TRF2 per cell was measured. Cell number >120. Values (mean ± SD) are from three independent experiments. ****, $p < 0.001$. (I) Immunoprecipitation of Myc-TRF2 in U2OS expressing YFP-ORCA WT or ΔSIM. The protein complex was analyzed by western blotting.

(J and K) (J) Representative images of immunofluorescence staining of TRF2 (red) and DNA (DAPI, blue) in HeLa 1.2.11 cells transiently expressing YFP-ORCA alone, YFP-ORCA with Myc-MMS21 WT or C215A (catalytically inefficient). Selected region of the merged image is shown as "Inset." Scale bar denotes 5 μm. (K) The percentages of YFP-ORCA foci co-localized with TRF2 per cell were measured. Cell number >150. Values (means ± SD) are from three independent experiments. *, $p < 0.05$. ***$p < 0.005$. ****, $p < 0.001$.

See also Figure S1.

association of HA-ORCA with telomere DNA (Figure S1P and S1Q) and attenuated the signal intensity of ORCA foci (Figure S1R and S1S). These results imply that shelterin components are required for the localization of ORCA to telomeres.

Shelterin complex is also present on telomeres of telomerase-positive cells. Therefore, we further addressed the mechanism by which ORCA is selectively localized to the ALT-telomeres. The shelterin components at ALT-telomeres are known to be SUMOylated by MMS21 SUMO ligase, and the inhibition of SUMOylation of Telomeric Repeat binding Factor 1 (TRF1) and TRF2 prevents APBs formation (Potts and Yu, 2007). To address whether the SUMOylation of shelterin complex influences the telomere localization of ORCA, we depleted MMS21 in U2OS cells and used immunoprecipitation and immunofluorescence staining to address the association of ORCA to shelterin/telomeres. We found that, in the absence of MMS21, the SUMOylation level of shelterin components decreased (Figures S1T–S1U) and the localization of ORCA to telomeres was severely compromised (Figures 1C and 1D). Furthermore, ORCA binding to the shelterin complex protein TRF2- and TRF1-Interacting Nuclear protein 2 (TIN2) was reduced (Figure 1E). Based on the prediction by GPS-SUMO (Zhao et al., 2014), ORCA contains three potential SUMO-Interacting Motifs (SIM) (Figure 1F). We mutated all the three SIM (ΔSIM) and evaluated the association of ORCA-ΔSIM to telomeres. As shown in Figures 1G–1I, the YFP-ORCA ΔSIM showed significantly reduced co-localization with telomeres and decreased interaction with TRF2. To further validate that the SUMOylation of shelterin components is crucial for ORCA enrichment at ALT-telomeres, we generated TRF1 and TRF2 mutants that cannot be SUMOylated (ΔSUMO) (Potts and Yu, 2007). As expected, the TRF1 and TRF2 ΔSUMO mutants interacted with ORCA less efficiently (Figures S1V–S1W). Furthermore, overexpression of MMS21 WT in HeLa 1.2.11 cells led to the SUMOylation of shelterin components (Figures 1X and 1Y) and the accumulation of ORCA at telomeres (Figures 1J and 1K), whereas the expression of MMS21 C215A, the E3 ligase-deficient mutant (Potts and Yu, 2005), leads to a less significant increase in ORCA association with telomeres (Figures 1J and 1K). All of these results suggest that the SUMOylation of shelterin components is crucial in the enrichment of ORCA at ALT-telomeres.

We have previously performed chromatin immunoprecipitation sequencing (ChIP-seq) in ALT-positive U2OS cells to identify ORCA-binding sites (Wang et al., 2017). It is interesting to note that >40% of ORCA peaks are within 10 Mb of the telomeres/subtelomeres, a region that denotes ∼14% of the genome (Figure 2A). Further mining of the ChIP-seq data revealed that ORCA is enriched at the subtelomeric regions of several chromosomes (namely, chr 7p, 8q, 13q, 17q, and 20q) and at almost all centromeres (Figures 2A, 2B, S2A, and S2B). ORCA is known to interact with the repressive histone marks, including H3K9me3 and H4K20me, and both these marks are enriched at telomeres and at subtelomeric regions (Vermeulen et al., 2010).

ORCA Is a Component of APBs and Negatively Regulates Homologous Recombination

One of the unique features of the ALT-positive cells is the presence of APBs, which by definition is the co-localization of PML nuclear bodies with telomeres (Yeager et al., 1999). APBs are dynamic and are cell cycle regulated (Jennifer et al., 2000). In addition to the single-stranded binding protein, RPA, and the key mediator of homologous recombination, RAD51, several other proteins involved in DNA repair and recombination are enriched in APB, including the components of MRN complex, WRN, and BLM (Bischof O et al., 2001; de Lange and Petrini, 2000; Hickson et al., 2001; Wu et al., 2000; Yeager et al., 1999; Zhu et al., 2000). We examined if ORCA was a component of the APB. PML and TRF2 staining in cells expressing YFP-ORCA revealed that ORCA was indeed a component of the APB (Figure 3A).

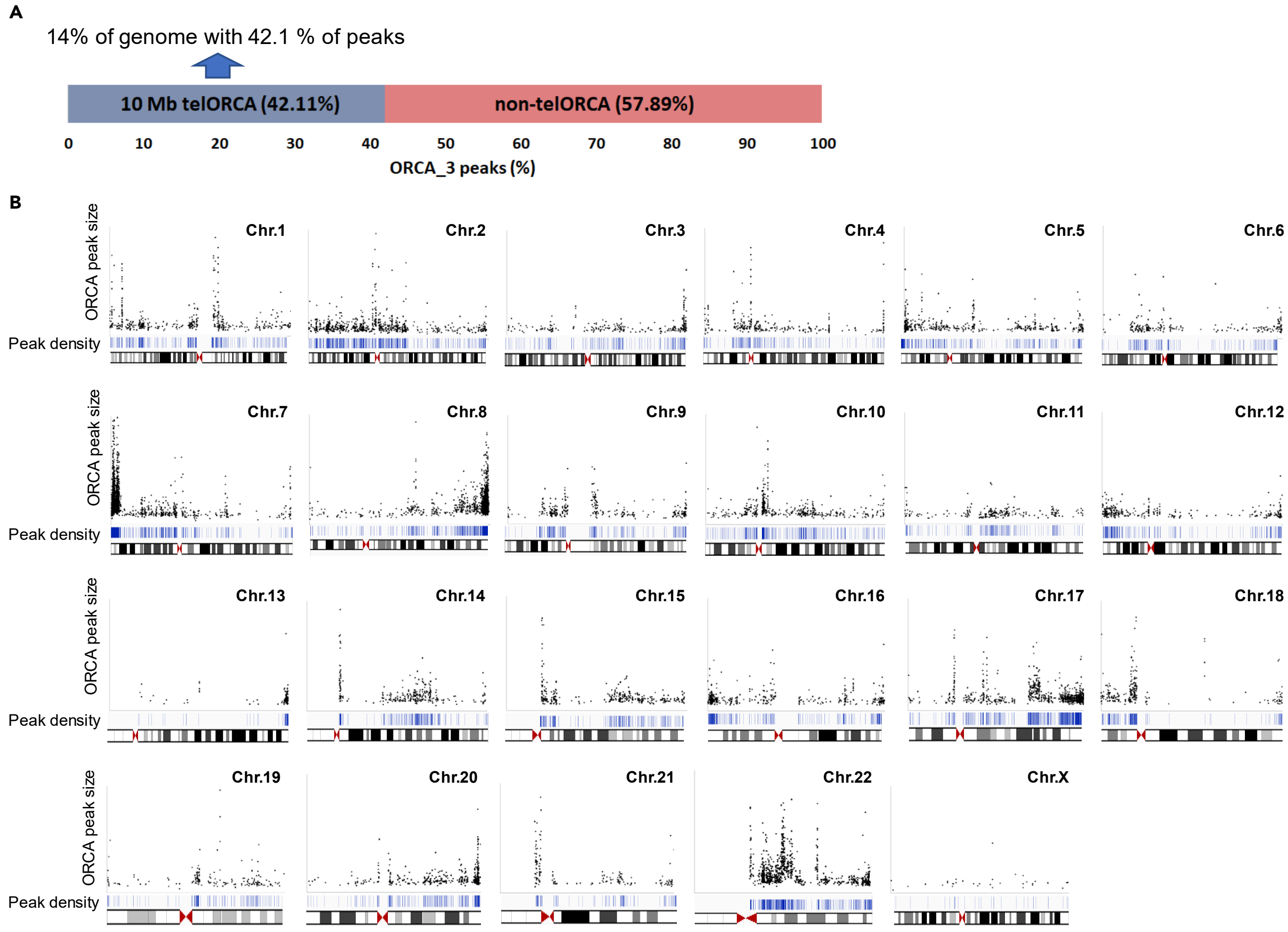

Figure 2. ORCA Is Enriched at the Subtelomeric Regions

(A) Distribution of ORCA ChIP-seq peaks in the genome (U2OS cells) (Wang et al., 2017). Note that 42.1% of the ORCA peaks are within 10 MB of telomeric regions.

(B) ORCA peak density (during mid-G1, 3 h after mitotic exit) across different chromosomes. For each chromosome, the dots represent ORCA peaks with x- and y-coordinates corresponding to the peak start position on chromosome and the peak size (bp), respectively. Images below dots graphs are composites from IGV screenshots with ORCA peak density in blue. Note the enrichment of ORCA at the subtelomeric regions, especially chromosomes 7p, 8q, 13q, 17q, and 20q and at the centromeric regions of most chromosomes.

See also Figure S2.

APBs have been considered both as a platform for telomere homologous recombination execution and also as a marker for ALT activity (Yeager et al., 1999). We found that, in the absence of ORCA, the number APBs per cell increased significantly (Figures 3B–3D and S3A–S3C). Overexpression of full-length ORCA (in the ORCA knockout [KO] background, please see the paragraph below for details) led to decrease in APB number, suggesting that ORCA prevented APB formation (Figure 3D). One interpretation of this result could be that ORCA plays a role in preventing homologous recombination and this could result in the reduction in the number of APBs (Figure 3D). In addition, we tested for non-replicative DNA synthesis with BrdU pulse labeling within APBs in cells lacking ORCA. To differentiate the S-phase cells from the non-S phase cells, the cells were enriched in G2 and we only evaluated the cells that displayed "non-replication patterns" of BrdU. We observed an increase in non-replicative DNA synthesis within APB of cells lacking ORCA, suggesting increased DNA repair process in ORCA-depleted cells (Figures S3D and S3E).

ORCA KO cells were generated in U2OS cells using CRISPR-mediated gene editing to validate results obtained by ORCA siRNA. ORCA KO cells grew at a slower rate in the first several passages but eventually proliferated at a rate similar to that of the control cells. In addition to increased APBs (Figure S3A), KO cells

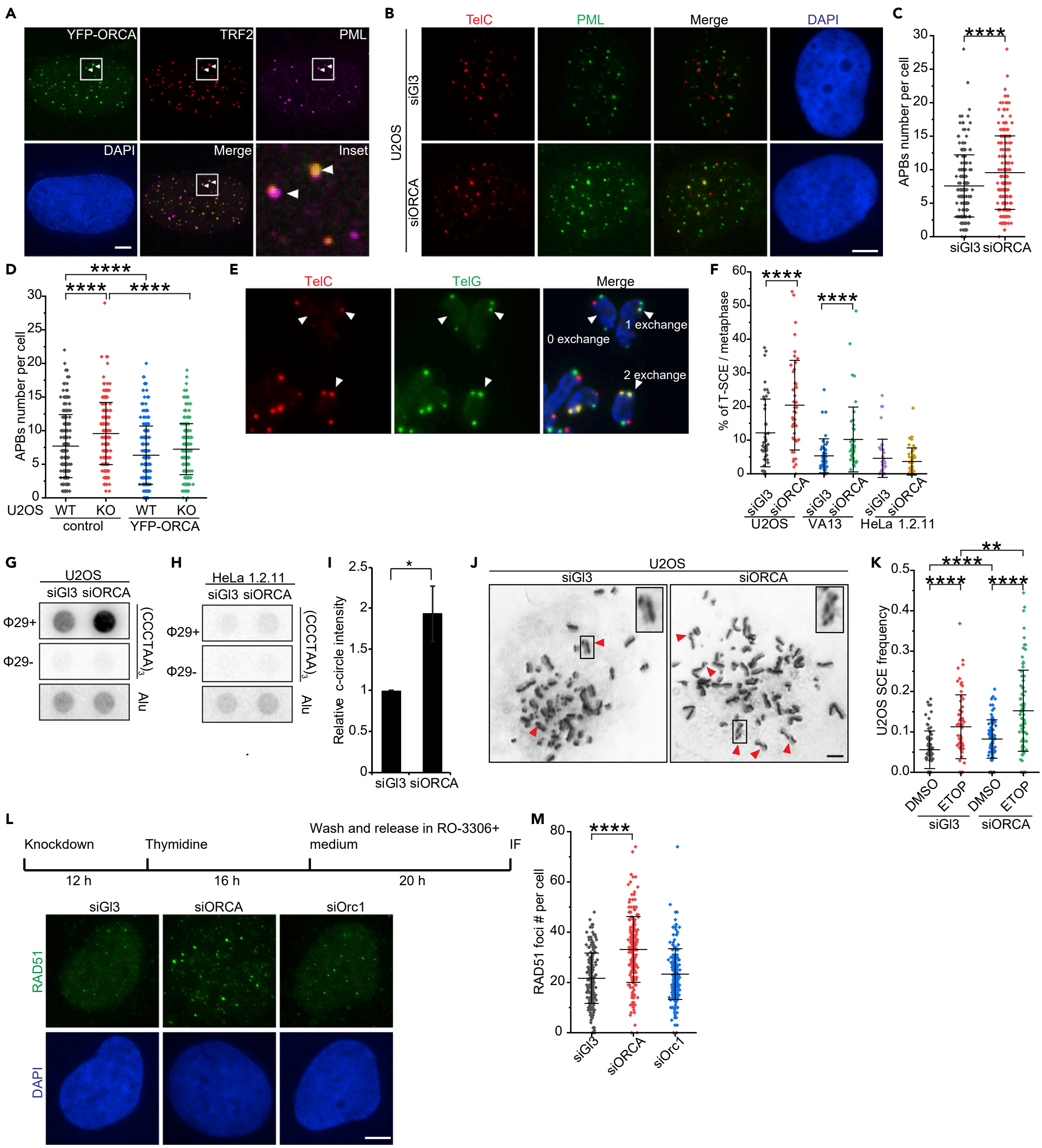

Figure 3. ORCA Is a Component of APBs and Loss of ORCA Results in Increased ALT Activity

(A) ORCA localizes within APBs. U2OS cells transiently expressing YFP-ORCA (green) were stained with TRF2 (red), PML (purple), and DNA (blue). APBs are defined as the co-localization of PML and TRF2. Selected regions of merged images are shown as "Insets." Arrowheads indicate ORCA positive APB. Scale bar denotes 5 μm.

(B and C) (B) Representative images of G2-enriched U2OS cells stained with PML (green), Telomere DNA (TelC, red), and DNA (DAPI, blue) in control (siGl3) and ORCA-depleted cells. Scale bar denotes 5 μm.

(C) Quantification of APBs number in U2OS cells treated with control or siORCA. APBs are defined as the co-localization of PML and TelC. Cell number >200. Values (means ± SD) are from three independent experiments. ****, $p < 0.001$.

Figure 3. *Continued*

(D) Quantification of APBs in U2OS WT or ORCA KO cells with or without YFP-ORCA transient expression. The number of APB per cell was measured. Cell number >150. Values (means ± SD) are from three independent experiments. ****, $p < 0.001$.

(E and F) (E) Representative image of telomere CO-FISH showing telomere sister chromatid exchange (T-SCE). Arrowheads indicate chromosome with zero exchange (upper left); one exchange (upper right); and two exchanges (bottom). (F) The percentages of T-SCE per metaphase spread were measured (metaphase spread N > 40) in U2OS, WI38-VA13, and HeLa 1.2.11 cells treated with control or siORCA. Values (means ± SD) are from three independent experiments. ****, $p < 0.001$.

(G–I) (G) Representative dot blot of c-circle in U2OS cells treated with control or siORCA. (H) Representative dot blot of c-circle in HeLa 1.2.11 cells treated with control or siORCA. (I) Quantification of c-circle level in U2OS cells treated with control or siORCA. The relative c-circle level is first normalized to loading control (Alu), then normalized to control. Values (mean ± SD) are from three independent experiments. *$p < 0.05$.

(J and K) (J) Representative images of harlequin chromosomes in U2OS cells treated with control or siORCA. Arrwoheads indicate chromosomes with Sister Chromatid Exchange. Scale bar denotes 5 μm. (K) Sister Chromatid Exchange (SCE) frequency (number of exchanges per chromosome number per metaphase spread) was measured in U2OS cells treated with control or siORCA, in the presence of DMSO or ETOP (5 μM) (Metaphase spread N > 60). Values (means ± SD) are from four independent experiments. **, $p < 0.01$, ****, $p < 0.001$.

(L and M) (L) Representative images of G2-enriched U2OS cells stained with RAD51 (green) and DAPI (DNA, blue). Scale bar denotes 5 μm. (M) The number of RAD51 foci per cell was measured. Cell number >200. ****, $p < 0.001$.

See also Figure S3.

of earlier passage showed defects in ORC loading, reduced MCM loading, and decreased proliferation rate (Figures S3F–S3K). Total levels of Orc2 also decreased in cells lacking ORCA (Figure S3I).

To address if ORCA controls homologous recombination at ALT-telomeres, we evaluated the frequency of telomere sister chromatid exchange (T-SCE) in the absence of ORCA (Figures 3E and 3F). We observed a consistent and significant increase in T-SCE in the absence of ORCA in ALT-positive cells (Figure 3F). The T-SCE frequency remained unaltered in ORCA-depleted telomerase-positive HeLa 1.2.11 (Figure 3F). The increase in APBs and T-SCE in the absence of ORCA suggests that ORCA could repress ALT activity. The c-circle assay is a rapid and quantitative method to measure changes in ALT activity and is now routinely used as a gold standard to determine the efficiency of ALT activity (Henson et al., 2009, 2017). The level of c-circle increased significantly in the absence of ORCA (Figures 3G–3I). The reduced ALT activity in the absence of ORCA suggests that ORCA suppresses homologous recombination at telomeres.

Since ORCA also localizes at non-telomeric regions in the genome (including centromeres and specific origins, Figure 2), and ORCA is highly enriched in testis, a tissue with high level of homologous recombination (Teng et al., 2010), we addressed if ORCA modulates homologous recombination at non-telomeric regions. We evaluated the level of sister chromatid exchange (SCE) (Figures 3J, 3K, S3L–S3M) and RAD51 foci formation (Figures 3L, 3M, S3N, and S3O) in the absence of ORCA. The increase in SCE and RAD51 foci in ORCA-depleted sample supported our model that ORCA acts as a negative regulator of homologous recombination not only at the telomeres but also globally. Because ORCA is known to form a complex with ORC, and ORC has been shown to localize to telomeres (Deng et al., 2007), we performed RAD51 staining upon Orc1 depletion as well. Interestingly, the depletion of Orc1 did not lead to a similar phenotype as that of ORCA depletion (Figures 3L, 3M), suggesting that the entire ORC may not be involved in modulating HR.

Because ORCA along with ORC controls replication initiation, the increase of RAD51 upon ORCA depletion (Figures 3L, 3M) could be the consequence of replication stress. We examined if the loss of ORCA caused DNA replication defects and replication stress at telomeres using Telomere DNA FISH. The frequency of telomere Signal Free Ends (SFE) and Fragile telomeres (FT) was determined (Figures S3P–S3R). Telomere Signal Free ends indicate loss of telomere protection, and Fragile Telomeres indicate replication stress at telomeres. The depletion of ORCA led to decreased SFE and no significant changes in FT (Figures S3P–S3R). Our previous study indicates that the ORCA association to heterochromatic regions is not necessarily facilitating the replication of these heterochromatic structures (Giri et al., 2015). However, given the heterogeneity at ALT-telomeres, the tendencies and the borderline results for the FTs, it is possible that ORCA is involved in the replication at ALT-telomeres.

ORCA Suppresses Homologous Recombination by Organizing Accurate Heterochromatin Architecture

One of the hallmarks of ALT-positive cells is that these cells utilize an HR-mediated mechanism to extend their telomeres. Intriguingly, ORCA was reported to be a substrate for ATM and ATR (Matsuoka et al., 2007), supporting our working model that ORCA might participate in HR. We observe that the telomeric sister chromatid exchange (T-SCE) is increased along with increased accumulation of RAD51 at the telomeres in the absence of ORCA. Furthermore, the number of APBs is significantly increased in the absence of ORCA, all pointing to a role of ORCA in influencing HR. There are at least two possible non-mutually exclusive explanations for elucidating the phenotypes observed in ORCA-depleted cells: (1) ORCA plays a direct role in modulating HR and (2) ORCA regulates heterochromatin organization at telomeres, and a decondensed chromatin at ALT-telomeres in the absence of ORCA results in increased HR.

We have previously shown that ORCA associates with the histone and DNA methylation machinery and orchestrates the establishment of a repressive chromatin environment (Giri et al., 2015; Giri and Prasanth, 2015; Wang et al., 2017). It is known that the disruption of DNA or histone methylation in mice causes an increase in telomere recombination and APB formation, implying that defects in heterochromatin formation provide an epigenetic basis for ALT (Benetti et al., 2007; Garcia-Cao et al., 2004; Gonzalo et al., 2006; O'Sullivan and Almouzni, 2014). To evaluate whether ORCA contributes to ALT by establishing the association of epigenetic marks at telomeric region, we quantified the levels of H3K9me3 in control and ORCA-depleted U2OS cells by H3K9me3 ChIP-seq analysis (Giri et al., 2015). We noted a global reduction in the distribution of H3K9me3 across the genome in ORCA-depleted cells in which approximately 50% reduction was observed at the subtelomeric regions (Figures 4A, S4A, and S4B). Telomeric ChIP results showed a decrease in H3K9me3 and marginally increased H4 acetylation at the telomeres in the absence of ORCA (Figures S4D and S4E). Changes observed upon ORCA depletion using the TelChIP assay represent the changes to all the telomeres of the population, whereas the H3K9me3 ChIP-seq enables us to visualize changes to individual subtelomeric regions. We also found increased TERRA RNA level in the telomeric regions of ORCA-depleted samples (Figures 4B–4E and S4C). It is interesting to note that ORCA is prominently enriched at chromosome 7p, and in its absence, the transcription of TERRA from this chromosome arm increases. These results point to an open chromatin environment in the absence of ORCA. These results suggest that ORCA-mediated heterochromatinization is critical and occurs in a context-dependent manner and it regulates various cellular processes.

ORCA Modulates RPA Binding to ssDNA

We next examined if ORCA associates with telomeres throughout the cell cycle or is enriched at telomeres at specific cell cycle stages. We found that ORCA associated with telomeres throughout interphase (G1, S, and G2) (Figures S5A–S5C). Interestingly, we found that ORCA interacted with one of the shelterin components, TPP1 in a cell-cycle-dependent manner, with maximum binding during mitosis and G1, gradually declining as cells entered S-phase (Figure 5A). Surprisingly, we found that ORCA interacted with the ssDNA-binding protein RPA, with maximal binding observed during G2 phase, at a time window when ORCA's interaction with TPP1 was found to be minimal (Figure 5A).

It is known that, during G2 phase, TPP1-POT1 heterodimer replaces the existing RPA from the newly synthesized telomere single-stranded overhangs (Flynn et al., 2011). In addition, TERRA and hnRNPA1 coordinate this RPA-to-POT1 switch on telomeric ssDNA (Flynn et al., 2011). This is required to prevent the activation of the Ataxia Telangiectasia and Rad3-related kinase (ATR) response (Flynn et al., 2012). To examine if ORCA participates in RPA replacement at telomeres during G2, ORCA- or Orc1- or TPP1-depleted cells were enriched at G2 and co-stained for TRF2 and RPA32 (Figures 5B–5D, S5D, and S5H). The depletion of ORCA in ALT cells led to significant increase in telomeric RPA-positive cells, whereas the depletion of Orc1 did not show significant differences from that of control (Figures 5B and 5C). A similar phenotype was also observed in ORCA KO U2OS cells (Figures S5E and S5F). The possible explanations for the increase of telomeric RPA include: defective TPP1-POT1 interaction with other shelterin components, defective RPA replacement by TPP1-POT1 heterodimer, or mis-regulation of RPA dissociation from telomeres. The interaction of TPP1 with other shelterin components was not affected in the absence of ORCA (Figure S5G). In addition, we did not observe an increase of telomeric RPA in ORCA-depleted HeLa cells (Figures 5D and S5H), indicating that the accumulation of telomeric RPA in the absence of ORCA was an ALT-specific phenotype.

To gain mechanistic insights into the function of ORCA at ALT-telomeres and to address why increased HR is observed in the absence of ORCA, we focused on uncovering the biological relevance of the interaction of ORCA with the ssDNA-binding protein RPA. Using purified RPA and ORCA, we found direct interaction between ORCA and RPA (Figure 5E), and such interaction between ORCA and RPA was also

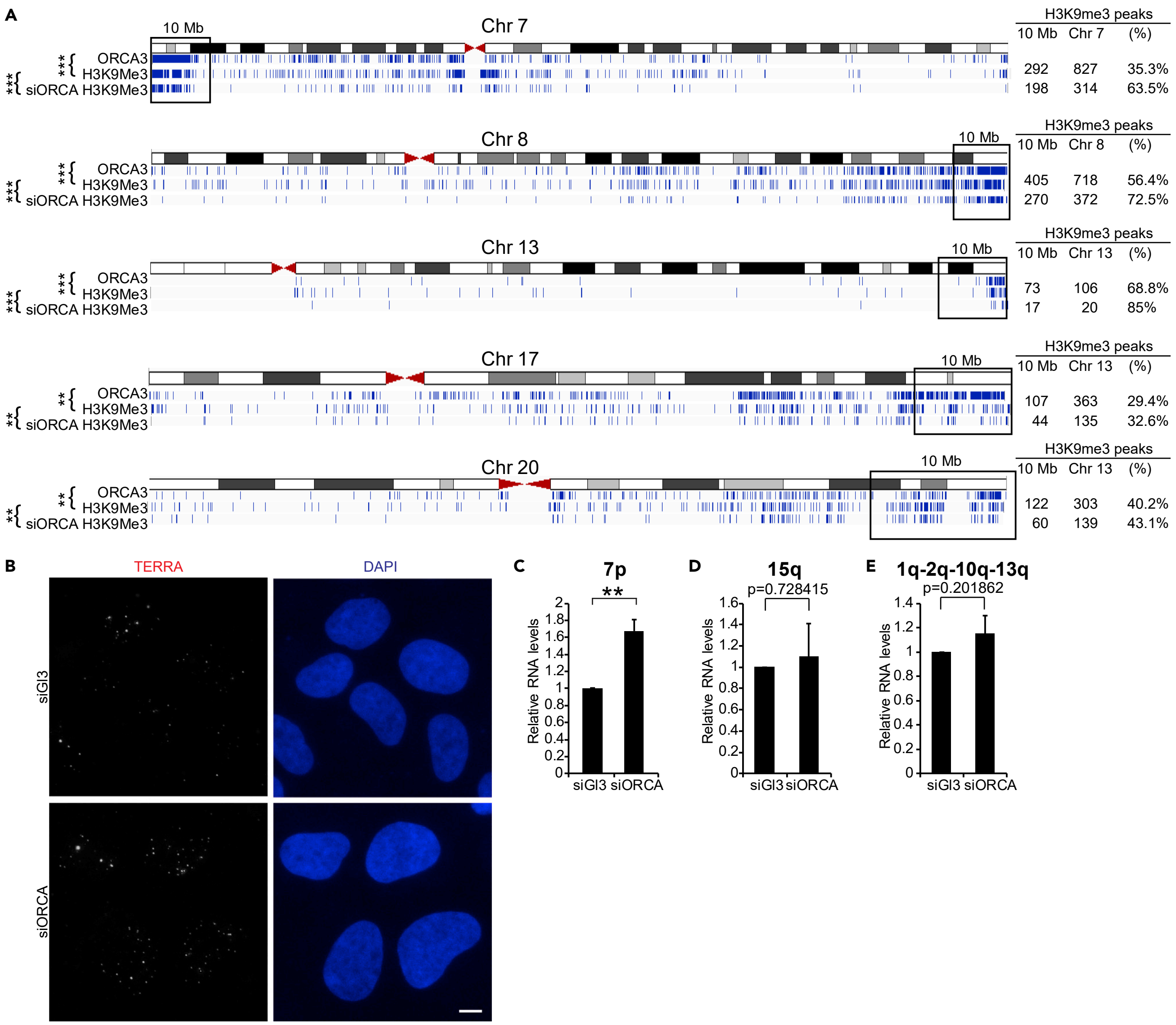

Figure 4. Depletion of ORCA Leads to Chromatin Decondensation

(A) Distribution of H3K9me3 ChIP-seq peaks in control and siORCA-treated U2OS cells. The numbers of H3K9Me3 peaks located in 10-Mb telomeric regions for Chr 7 p arm, Chr 8, 13, 17, 20 q arms (black rectangles) as well as the numbers of peaks in entire chromosomes are shown on the right. The proportions of peaks in telomeric regions relative to entire chromosomes are displayed as percentages (right). Note the global reduction as well as reduction of H3K9me3 marks at subtelomeric regions. Pearson's correlations between ORCA and H3K9Me3 peak distributions in 10-Mb sections along chromosomes 7, 8, 13, 17, and 20 in control and siORCA cells were calculated using GraphPad Prism. *** denotes $p < 0.0001$; ** denotes $p < 0.001$.

(B) Representative images of U2OS cells treated with control or siORCA. Cells were stained with TERRA RNA and DNA (DAPI, blue). Scale bar denotes 5 μm.

(C–E) Quantification of relative TERRA level transcribed from 7p (C), 15q (D), and 1q-2q-10q-13q (E) in control or siORCA-treated sample. Values (mean ± SD) are from three independent experiments. $^{**}p < 0.01$.

See also Figure S4.

validated by SiMPull analysis (Figures 5F–5H). To address if ORCA could modulate the binding of RPA to ssDNA, we first incubated RPA with telomeric ssDNA [$(TTAGGG)_8$] and then incubated with increasing levels of purified GST-ORCA (Figure 5I) or an ORC subunit (GST-Orc6) (Figure S5I) and determined the binding affinity of RPA to ssDNA. We found that, as the amounts of ORCA increased, the binding of RPA to ssDNA declined (Figure 5I). This was not the case when GST-Orc6 was used (Figure S5I). These results were corroborated by *in vivo* imaging experiments, where we found that the intensity of RPA at a nuclear locus was inversely proportional to the amount of ORCA (Figures 5J and S5J). Our results suggest

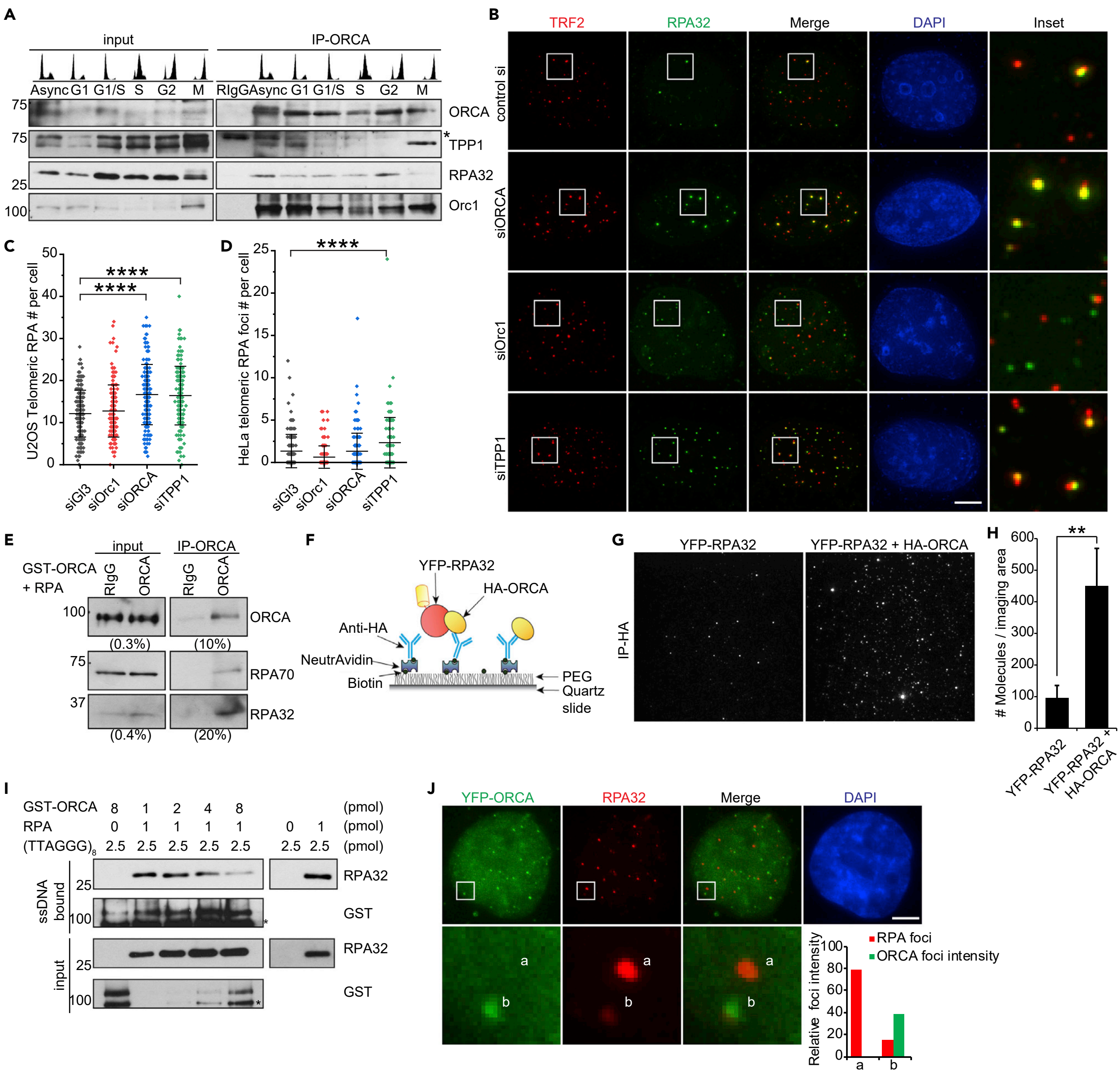

Figure 5. ORCA Associates with RPA and Modulates the Binding of RPA to ssDNA

(A) Immunoprecipitation using ORCA antibody in U2OS cells synchronized at different stages of the cell cycle, namely, G1, G1/S, S, G2, and M. Flow cytometry profiles are shown on top of the panel. Immunoblotting of ORCA, TPP1, RPA32, and Orc1 are shown. '*' denotes cross-reacting band.

(B and C) (B) Immunolocalization of RPA (RPA32, green) to telomeres (TRF2, red) in control and siORC1-, siORCA-, siTPP1-treated U2OS cells during G2 phase. Telomeric RPA is defined as RPA foci that co-localized with TRF2 signal. Selected regions of the merged images are shown as "Insets." Scale bar denotes 5 μm. (C) The number of telomeric RPA per cell was measured. Cell number >170. Values (means $\pm$ SD) are from three independent experiments. ****, $p < 0.001$.

(D) The same experiment as described in (B) was conducted in HeLa cells, and the number of telomeric RPA per cell was measured. Cell number >150. Values (means $\pm$ SD) are from three independent experiments. ****, $p < 0.001$. (E) Direct interaction of purified ORCA and RPA. The protein complex was analyzed by western blotting.

(F–H) (F) Schematic of SiMPull assay for ORCA-RPA32 interaction. (G) Total internal reflection fluorescence (TIRF) images of YFP-molecules pulled down from U2OS cell lysates expressing HA-ORCA and YFP-RPA32 using biotinylated HA antibody. YFP-RPA32 alone was used as the negative control. (H) Average number of YFP fluorescent molecules per imaging area (5,000 μm^2). Values (means $\pm$ SD) are from three independent experiments. **, $p < 0.01$.

Figure 5. *Continued*

(I) Biotinylated $(TTAGGG)_8$ pull-down assay using purified ORCA and RPA. The amount of ssDNA-binding proteins was analyzed using western blotting. '*' denotes cross-reacting band.

(J) Representative images of U2OS transiently expressed YFP-ORCA WT stained with RPA32 (red) and DNA (DAPI, blue). Scale bar denotes 5 μm. The signal intensity of YFP-ORCA and RPA32 in the selected region was plotted.

See also Figure S5.

that ORCA and RPA are in a complex and that ORCA modulates RPA binding to chromatin. This would explain why in the absence of ORCA there is increased RPA at telomeres.

We propose that ORCA is important for chromatin condensation and the increased concentration of ORCA at the ALT-telomeres functions as a negative regulator of homologous recombination by facilitating heterochromatin organization and disrupting RPA binding to the ssDNA (Figure 6).

DISCUSSION

ORC and ORCA are multifunctional replication initiator proteins and play diverse roles in cell-cycle progression. ORCA coordinates with histone and DNA methylation machinery to establish a repressive chromatin environment at a subset of DNA replication origins, and this is critical for priming these for replication late in S-phase (Wang et al., 2017). Both ORC and ORCA associate with heterochromatin, including at telomeres and centromeres, yet their molecular roles in orchestrating telomere maintenance and chromosome segregation remain to be understood. We demonstrate that ORCA is enriched at telomeres of cells that utilize ALT mechanism to extend their telomeres. However, the molecular function of ORCA at the telomeres is unknown. Telomeres of ALT-positive cells are quite different from those of telomerase-positive cells. Several hallmarks of ALT-positive cells include long and heterogeneous telomeres length, variant telomere sequences, extra-chromosomal telomeric repeat DNA, ALT-associated PML bodies, increased H3K79me2 at sub-telomere regions, and increased TERRA accumulation (Dilley and Greenberg, 2015; O'Sullivan and Almouzni, 2014; Pickett and Reddel, 2015). We observe that the SUMOylation of shelterin components by MMS21 is required for ORCA enrichment at ALT-telomeres. Without the shelterin or the SUMO ligase, ORCA shows diminished association to telomeres.

ALT cells utilize homologous recombination to maintain their telomere length. The exact molecular mechanism and all the factors that dictate ALT-telomere maintenance remain elusive. Genome-wide binding of ORCA in ALT cells showed enrichment of ORCA at specific sub-telomeres, specifically chromosomes 7p, 8q, 13q, 17q, and 20q. One common feature of all these telomeres is the enrichment of H3K9me3 mark at the telomeres. Chromosome ends 7 and 8 also showed enrichment for fragile sites, regions commonly known for active HR. ALT-telomeres have a more open chromatin as compared with telomerase-positive cells (Episkopou et al., 2014). This is correlated with reduced DNA methylation and H3K9me3 with a concomitant increase in TERRA levels. We observe that, in the absence of ORCA, H3K9me3 levels decline even further causing chromatin decompaction. This is accompanied by increased levels of TERRA RNA, specifically from chromosomes that are known to be enriched for ORCA, suggesting that, upon loss of ORCA, chromatin decompaction enables TERRA transcription. Furthermore, elevated telomeric recombination and APBs formation support the defects in heterochromatin formation, similar to what has been reported in mice when DNA and histone methyltransferases are depleted (Benetti et al., 2007; Garcia-Cao et al., 2004; Gonzalo et al., 2006).

ORCA associates with SUMOylated shelterin at telomeres; at the same time, ORCA can also associate with methylated histones and methylated DNA. The enrichment of ORCA at specific ALT-telomeres may also be mediated by its binding to the non-coding RNA TERRA, which itself is significantly upregulated in ALT cells and is known to be transcribed from select telomeres, including but not limited to chromosome 20 (Montero et al., 2016). 20q-TERRAs have been shown to be essential for the establishment of H3K9me3, H4K20me3, and H3K27me3 (Montero et al., 2018). A recent study has pointed that TERRA associates with ORC and ORCA (Chu et al., 2017). TERRA transcription has also been implicated in telomere instability and recombination in ALT cells (Arora et al., 2014).

We found that ORCA also directly binds to the single-stranded DNA-binding protein RPA. Once ORCA associates with RPA, it modulates RPA binding to ssDNA. The binding of RPA to ssDNA is the critical first step in HR-mediated repair. We find that, in cells lacking ORCA, the RPA as well as RAD51 association to telomeres is elevated. We propose that ORCA binds to RPA and regulates its binding to ssDNA. Once

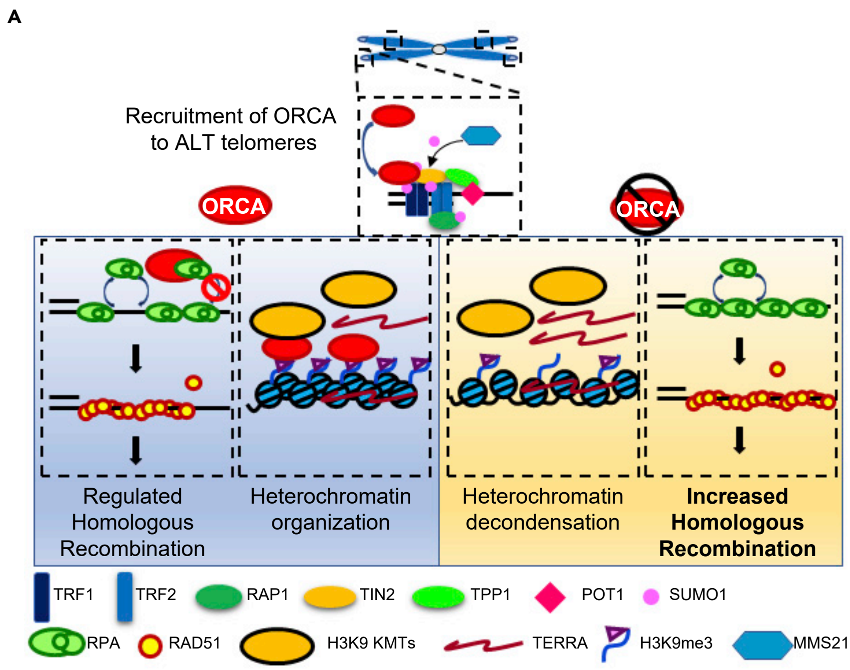

Figure 6. ORCA/LRWD1 Regulates Homologous Recombination at ALT-telomeres by Modulating RPA binding to ssDNA and Heterochromatin Organization

Schematic representation of ORCA recruitment to ALT-telomeres and its role in preventing unsolicited homologous recombination by modulating chromatin architecture and RPA association.

the levels of ORCA start to increase at telomeres, it titrates RPA away from ssDNA by sponging it. Therefore, in the absence of ORCA, more RPA binds to ssDNA, enabling RAD51 assembly, resulting in increased HR, as is evident by increased T-SCE, SCE, and RAD51 foci. Alternative model posits that, in the absence of ORCA, increased chromatin decompaction facilitates the loading of factors, including RPA that enables HR. This is consistent with the working model that the compact chromatin at telomeres is inaccessible to nucleases and other factors that stimulate HR (Bao and Shen, 2007; Mao et al., 2016; Murr et al., 2006).

RPA is also known to mediate recombination repair when the cells encounter replication stress caused by replication fork stalling. We find that the levels of ORCA are the lowest during S phase of the cell cycle, suggesting that the downregulation of ORCA is critical to initiate HR whenever a cell confronts a replication stress in the form of stalled fork. This could be either through its role in chromatin organization or through its direct binding to RPA to modulate its binding and activity. This is consistent with our results that ORCA inhibits HR not only at ALT-telomeres but also at other genomic sites. Intriguingly, several subunits of ORC and ORCA were reported to be a substrate for ATM and ATR (Matsuoka et al., 2007), supporting our model that these proteins participate in HR.

Diverse cellular pathways function coordinately to mitigate replication stress at telomeres to ensure accurate replication fork progression and DNA double-strand break repair. Because ALT-telomeres have relatively open chromatin configuration, they are susceptible to increased replication stress. We find that, in the absence of ORCA, there is increased BrdU incorporation at the APB consistent with increased DNA repair. APBs are known to assemble at telomeres to induce DNA repair process (Chung et al., 2011). Recent studies on several cellular factors that specifically associate with ALT-telomeres are beginning to provide important insights into the mechanisms that govern telomere maintenance in ALT cells. We have found that the replication initiator protein ORCA associates with ALT-telomeres and the loss of ORCA results in hyper-ALT phenotype. This is similar to the loss of FANCD2 in ALT cells, a component of the APB, the loss of which shows an increase in recombination by-products and has been implicated in promoting intramolecular resolution of stalled replication forks in telomeric DNA (Root et al., 2016). Similar phenotype has also been observed upon depletion of SMARCAL1 (Cox et al., 2016), a factor that associates with telomeric DNA in ALT cells and functions to resolve replication stress and enable telomere elongation (Cox et al., 2016). Also, the expression of SLX4 endonuclease represses ALT-mediated telomere elongation by allowing the telomeric recombination intermediates to resolve after strand invasion (Sobinoff et al., 2017). ORCA inhibits HR at ALT-telomeres by at least two modes: (1) by facilitating heterochromatinization at ALT-telomeres and (2) by directly binding to RPA and modulating its association to ssDNA. Although these two modes of action are true for other genomic sites as well, future work will entail understanding the precise pathway and how ORCA associates with specific protein partners to maintain genome stability.

Limitations of the Study

We acknowledge that there are limitations to the findings of the present study. First, the molecular mechanism of how ORCA controls RPA binding to ssDNA remains to be determined. It will be interesting to investigate whether ORCA competes with RPA for ssDNA or the binding of ORCA to RPA alters the DNA binding affinity of RPA. Second, the functional relevance of ORCA enrichment at select telomeres remains unknown. ALT-positive cells in general display heterogeneous telomere length. Because ORCA is enriched only at specific telomeres in ALT cells, it was difficult to ascertain the overall change in telomere length upon ORCA depletion. Finally, during mitosis, ORCA is enriched at centromeres and continues to localize at select telomeres. Future work will determine if ORCA has a direct role in mitosis or if there is clustering of origins at centromeres and telomeres during mitosis.

METHODS

All methods can be found in the accompanying Transparent Methods supplemental file.

DATA AND CODE AVAILABILITY

H3K9me3 ChIP-seq are available at http://www.ncbi.nlm.nih.gov/geo/query/acc.cgi?acc=GSE68129, and the ORCA ChIP-seq in U2OS cells are available at GSE81165.

SUPPLEMENTAL INFORMATION

Supplemental Information can be found online at https://doi.org/10.1016/j.isci.2020.101038.

ACKNOWLEDGMENTS

We thank members of the Prasanth laboratory for discussions and suggestions. We thank Drs. A. Chakraborty, T. deLange, R. Flynn, R. Greenberg, C. Mizzen, C. Prives, Z. Shen, B. Stillman, L. Zou, and V. Mohan for providing reagents and suggestions. We thank Dr. D. Rivier and Ms. Adusumilli for critical reading of the manuscript. We thank Dr. Lorinc Pongor for advice on statistical analysis of sequencing data. This work was supported by NSF-CMMB-IGERT fellowship to R.Y.C.H.; The Intramural Program of the National Cancer Institute, Center for Cancer Research (1ZIABC010419 to M.I.A.), National Institutes of Health (R21AG065748), National Science Foundation EAGER (MCB 1723008) and Cancer Center at Illinois Seed Grant and Prairie Dragon Paddlers awards to K.V.P., and NSF (1243372 and 1818286) and NIH (GM099669 and GM125196) awards to S.G.P. T.H. is an investigator with Howard Hughes Medical Institute. The authors declare no competing financial interests.

AUTHOR CONTRIBUTIONS

R.Y.C.H. designed, performed, and analyzed most experiments. Y.-C.L. and Y.W. helped purify proteins; C.R. and M.I.A. analyzed the ChIP-seq data; Q.S. performed TERRA qPCR. D.K.S. generated the ORCA KO cell line; B.M. provided reagents and assisted with generating ORCA KO cell line; V.A. and J.M. helped with SiMPull experiments; A.M. helped with cloning. T.H. provided technical support and conceptual advice toward SiMPull experiments. S.G.P. and K.V.P. supervised the project. S.G.P. and R.Y.C.H. wrote the manuscript.

DECLARATION OF INTERESTS

The authors declare no competing interests.

Received: October 18, 2019
Revised: March 26, 2020
Accepted: April 1, 2020
Published: May 22, 2020

REFERENCES

Arnoult, N., Van Beneden, A., and Decottignies, A. (2012). Telomere length regulates TERRA levels through increased trimethylation of telomeric H3K9 and HP1alpha. Nat. Struct. Mol. Biol. *19*, 948–956.

Arora, R., Lee, Y., Wischnewski, H., Brun, C.M., Schwarz, T., and Azzalin, C.M. (2014). RNaseH1 regulates TERRA-telomeric DNA hybrids and telomere maintenance in ALT tumour cells. Nat. Commun. *5*, 5220.

Azzalin, C.M., Reichenbach, P., Khoriauli, L., Giulotto, E., and Lingner, J. (2007). Telomeric repeat containing RNA and RNA surveillance factors at mammalian chromosome ends. Science *318*, 798–801.

Bao, Y., and Shen, X. (2007). Chromatin remodeling in DNA double-strand break repair. Curr. Opin. Genet. Dev. *17*, 126–131.

Bartke, T., Vermeulen, M., Xhemalce, B., Robson, S.C., Mann, M., and Kouzarides, T. (2010). Nucleosome-interacting proteins regulated by DNA and histone methylation. Cell *143*, 470–484.

Bell, S.P., and Dutta, A. (2002). DNA replication in eukaryotic cells. Annu. Rev. Biochem. *71*, 333–374.

Bell, S.P., and Stillman, B. (1992). ATP-dependent recognition of eukaryotic origins of DNA replication by a multiprotein complex. Nature *357*, 128–134.

Benetti, R., Gonzalo, S., Jaco, I., Schotta, G., Klatt, P., Jenuwein, T., and Blasco, M.A. (2007). Suv4-20h deficiency results in telomere elongation and derepression of telomere recombination. J. Cell Biol. *178*, 925–936.

Bischof O, K.S.-H., Irving, J., Beresten, S., Ellis, N.A., and Campisi, J. (2001). Regulation and localization of the bloom syndrome protein in response to DNA damage. J. Cell Biol. *153*, 367–380.

Blasco, M.A. (2007). The epigenetic regulation of mammalian telomeres. Nat. Rev. Genet. *8*, 299–309.

Blow, J.J., and Tanaka, T.U. (2005). The chromosome cycle: coordinating replication and segregation. Second in the cycles review series. EMBO Rep. *6*, 1028–1034.

Bryan, T.M., Englezou, A., Gupta, J., Bacchetti, S., and Reddel, R.R. (1995). Telomere elongation in immortal human cells without detectable telomerase activity. EMBO J. *14*, 4240–4248.

Cesare, A.J., and Griffith, J.D. (2004). Telomeric DNA in ALT cells is characterized by free telomeric circles and heterogeneous t-loops. Mol. Cell Biol. *24*, 9948–9957.

Chu, H.P., Cifuentes-Rojas, C., Kesner, B., Aeby, E., Lee, H.G., Wei, C., Oh, H.J., Boukhali, M., Haas, W., and Lee, J.T. (2017). TERRA RNA antagonizes ATRX and protects telomeres. Cell *170*, 86–101 e116.

Chung, I., Leonhardt, H., and Rippe, K. (2011). De novo assembly of a PML nuclear subcompartment occurs through multiple pathways and induces telomere elongation. J. Cell Sci. *124*, 3603–3618.

Cox, K.E., Marechal, A., and Flynn, R.L. (2016). SMARCAL1 resolves replication stress at ALT telomeres. Cell Rep. *14*, 1032–1040.

Craig, J.M., Earle, E., Canham, P., Wong, L.H., Anderson, M., and Choo, K.H. (2003). Analysis of mammalian proteins involved in chromatin modification reveals new metaphase centromeric proteins and distinct chromosomal distribution patterns. Hum. Mol. Genet. *12*, 3109–3121.

Deng, Z., Dheekollu, J., Broccoli, D., Dutta, A., and Lieberman, P.M. (2007). The origin recognition complex localizes to telomere repeats and prevents telomere-circle formation. Curr. Biol. *17*, 1989–1995.

Deng, Z., Norseen, J., Wiedmer, A., Riethman, H., and Lieberman, P.M. (2009). TERRA RNA binding to TRF2 facilitates heterochromatin formation and ORC recruitment at telomeres. Mol. Cell *35*, 403–413.

Dilley, R.L., and Greenberg, R.A. (2015). ALTernative telomere maintenance and cancer. Trends Cancer *1*, 145–156.

Episkopou, H., Draskovic, I., Van Beneden, A., Tilman, G., Mattiussi, M., Gobin, M., Arnoult, N., Londono-Vallejo, A., and Decottignies, A. (2014). Alternative Lengthening of Telomeres is characterized by reduced compaction of telomeric chromatin. Nucleic Acids Res. *42*, 4391–4405.

Flynn, R.L., Centore, R.C., O'Sullivan, R.J., Rai, R., Tse, A., Songyang, Z., Chang, S., Karlseder, J., and Zou, L. (2011). TERRA and hnRNPA1 orchestrate an RPA-to-POT1 switch on telomeric single-stranded DNA. Nature *471*, 532–536.

Flynn, R.L., Chang, S., and Zou, L. (2012). RPA and POT1: friends or foes at telomeres? Cell Cycle *11*, 652–657.

Garcia-Cao, M., O'Sullivan, R., Peters, A.H., Jenuwein, T., and Blasco, M.A. (2004). Epigenetic regulation of telomere length in mammalian cells by the Suv39h1 and Suv39h2 histone methyltransferases. Nat. Genet. *36*, 94–99.

Giri, S., Aggarwal, V., Pontis, J., Shen, Z., Chakraborty, A., Khan, A., Mizzen, C., Prasanth, K.V., Ait-Si-Ali, S., Ha, T., et al. (2015). The preRC protein ORCA organizes heterochromatin by assembling histone H3 lysine 9 methyltransferases on chromatin. Elife *4*, https://doi.org/10.7554/eLife.06496.

Giri, S., and Prasanth, S.G. (2015). Association of ORCA/LRWD1 with repressive histone methyl transferases mediates heterochromatin organization. Nucleus *6*, 435–441.

Gonzalo, S., Jaco, I., Fraga, M.F., Chen, T., Li, E., Esteller, M., and Blasco, M.A. (2006). DNA methyltransferases control telomere length and telomere recombination in mammalian cells. Nat. Cell Biol. *8*, 416–424.

Henson, J.D., Cao, Y., Huschtscha, L.I., Chang, A.C., Au, A.Y., Pickett, H.A., and Reddel, R.R. (2009). DNA C-circles are specific and quantifiable markers of alternative-lengthening-of-telomeres activity. Nat. Biotechnol. *27*, 1181–1185.

Henson, J.D., Lau, L.M., Koch, S., Martin La Rotta, N., Dagg, R.A., and Reddel, R.R. (2017). The C-Circle Assay for alternative-lengthening-of-telomeres activity. Methods *114*, 74–84.

Hickson, I.D., Davies, S.L., Li, J.-L., Levitt, N.C., Mohaghegh, P., North, P.S., and Wu, L. (2001). Role of the Bloom's syndrome helicase in maintenance of genome stability. Biochem. Soc. Trans. *29* (Pt 2), 201–204.

Jennifer, V., Grobelny, A.K.G., and Dominique Broccoli. (2000). ALT-associated PML bodies are present in viable cells and are enriched in cells in the G2/M phase of the cell cycle. J. Cell Sciene *113*, 4577–4585.

de Lange, T., and Petrini, J.H. (2000). A new connection at human telomeres association of the Mre11 complex with TRF2. Cold Spring Harb. Perspect. Biol. *65*, 265–273.

Loayza, D., and De Lange, T. (2003). POT1 as a terminal transducer of TRF1 telomere length contrl. Nature *423*, 1013–1018.

Londoño-Vallejo, J.A., Der-Sarkissian, H., Cazes, L., Bacchetti, S., and Reddel, R.R. (2004). Alternative lengthening of telomeres is characterized by high rates of telomeric exchange. Cancer Res. *64*, 2324–2327.

Mao, P., Liu, J., Zhang, Z., Zhang, H., Liu, H., Gao, S., Rong, Y.S., and Zhao, Y. (2016). Homologous recombination-dependent repair of telomeric DSBs in proliferating human cells. Nat. Commun. *7*, 12154.

Matsuoka, S., Ballif, B.A., Smogorzewska, A., McDonald, E.R., 3rd, Hurov, K.E., Luo, J., Bakalarski, C.E., Zhao, Z., Solimini, N., Lerenthal, Y., et al. (2007). ATM and ATR substrate analysis reveals extensive protein networks responsive to DNA damage. Science *316*, 1160–1166.

Montero, J.J., Lopez de Silanes, I., Grana, O., and Blasco, M.A. (2016). Telomeric RNAs are essential to maintain telomeres. Nat. Commun. *7*, 12534.

Montero, J.J., Lopez-Silanes, I., Megias, D., F Fraga, M., Castells-Garcia, A., and Blasco, M.A. (2018). TERRA recruitment of polycomb to telomeres is essential for histone trymethylation marks at telomeric heterochromatin. Nat. Commun. *9*, 1548.

Murnane, J.P., Sabatier, L., Marder, B.A., and Morgan, W.F. (1994). Telomere dynamics in an immortal human cell line. EMBO J. *13*, 4953–4962.

Murr, R., Loizou, J.I., Yang, Y.G., Cuenin, C., Li, H., Wang, Z.Q., and Herceg, Z. (2006). Histone acetylation by Trrap-Tip60 modulates loading of repair proteins and repair of DNA double-strand breaks. Nat. Cell Biol. *8*, 91–99.

O'Sullivan, R.J., and Almouzni, G. (2014). Assembly of telomeric chromatin to create ALTernative endings. Trends Cell Biol. *24*, 675–685.

Ohta, S., Bukowski-Wills, J.C., Sanchez-Pulido, L., Alves Fde, L., Wood, L., Chen, Z.A., Platani, M., Fischer, L., Hudson, D.F., Ponting, C.P., et al.

(2010). The protein composition of mitotic chromosomes determined using multiclassifier combinatorial proteomics. Cell *142*, 810–821.

Pickett, H.A., and Reddel, R.R. (2015). Molecular mechanisms of activity and derepression of alternative lengthening of telomeres. Nat. Struct. Mol. Biol. *22*, 875–880.

Potts, P.R., and Yu, H. (2005). Human MMS21/NSE2 is a SUMO ligase required for DNA repair. Mol. Cell Biol. *25*, 7021–7032.

Potts, P.R., and Yu, H. (2007). The SMC5/6 complex maintains telomere length in ALT cancer cells through SUMOylation of telomere-binding proteins. Nat. Struct. Mol. Biol. *14*, 581–590.

Prasanth, S.G., Prasanth, K.V., and Stillman, B. (2002). Orc6 involved in DNA replication, chromosome segregation, and cytokinesis. Science *297*, 1026–1031.

Prasanth, S.G., Prasanth, K.V., Siddiqui, K., Spector, D.L., and Stillman, B. (2004). Human Orc2 localizes to centrosomes, centromeres and heterochromatin during chromosome inheritance. EMBO J. *23*, 2651–2663.

Prasanth, S.G., Shen, Z., Prasanth, K.V., and Stillman, B. (2010). Human origin recognition complex is essential for HP1 binding to chromatin and heterochromatin organization. Proc. Natl. Acad. Sci. U S A *107*, 15093–15098.

Root, H., Larsen, A., Komosa, M., Al-Azri, F., Li, R., Bazett-Jones, D.P., and Stephen Meyn, M. (2016). FANCD2 limits BLM-dependent telomere instability in the alternative lengthening of telomeres pathway. Hum. Mol. Genet. *25*, 3255–3268.

Sasaki, T., and Gilbert, D.M. (2007). The many faces of the origin recognition complex. Curr. Opin. Cell Biol. *19*, 337–343.

Schoeftner, S., and Blasco, M.A. (2008). Developmentally regulated transcription of mammalian telomeres by DNA-dependent RNA polymerase II. Nat. Cell Biol. *10*, 228–236.

Shen, Z., Sathyan, K.M., Geng, Y., Zheng, R., Chakraborty, A., Freeman, B., Wang, F., Prasanth, K.V., and Prasanth, S.G. (2010). A WD-repeat protein stabilizes ORC binding to chromatin. Mol. Cell *40*, 99–111.

Shen, Z., Chakraborty, A., Jain, A., Giri, S., Ha, T., Prasanth, K.V., and Prasanth, S.G. (2012). Dynamic association of ORCA with prereplicative complex components regulates DNA replication initiation. Mol. Cell Biol. *32*, 3107–3120.

Sobinoff, A.P., Allen, J.A., Neumann, A.A., Yang, S.F., Walsh, M.E., Henson, J.D., Reddel, R.R., and Pickett, H.A. (2017). BLM and SLX4 play opposing roles in recombination-dependent replication at human telomeres. EMBO J. *36*, 2907–2919.

Stillman, B. (2005). Origin recognition and the chromosome cycle. FEBS Lett. *579*, 877–884.

Takai, K.K., Hooper, S., Blackwood, S., Gandhi, R., and de Lange, T. (2010). In vivo stoichiometry of shelterin components. J. Biol. Chem. *285*, 1457–1467.

Tatsumi, Y., Ezura, K., Yoshida, K., Yugawa, T., Narisawa-Saito, M., Kiyono, T., Ohta, S., Obuse, C., and Fujita, M. (2008). Involvement of human ORC and TRF2 in pre-replication complex assembly at telomeres. Genes Cells *13*, 1045–1059.

Teng, Y.N., Liao, M.H., Lin, Y.B., Kuo, P.L., and Kuo, T.Y. (2010). Expression of lrwd1 in mouse testis and its centrosomal localization. Int. J. Androl. *33*, 832–840.

Vermeulen, M., Eberl, H.C., Matarese, F., Marks, H., Denissov, S., Butter, F., Lee, K.K., Olsen, J.V., Hyman, A.A., Stunnenberg, H.G., et al. (2010). Quantitative interaction proteomics and genome-wide profiling of epigenetic histone marks and their readers. Cell *142*, 967–980.

Victoria Lundblad, E.H.B. (1993). An alternative pathway for yeast telomere maintenance rescues est1 senescence. Cell *73*, 347–360.

Wang, Y., Khan, A., Marks, A.B., Smith, O.K., Giri, S., Lin, Y.C., Creager, R., MacAlpine, D.M., Prasanth, K.V., Aladjem, M.I., et al. (2017). Temporal association of ORCA/LRWD1 to late-firing origins during G1 dictates heterochromatin replication and organization. Nucleic Acids Res. *45*, 2490–2502.

Wu, G., Lee, W.H., and Chen, P.L. (2000). NBS1 and TRF1 colocalize at promyelocytic leukemia bodies during late S/G2 phases in immortalized telomerase-negative cells. Implication of NBS1 in alternative lengthening of telomeres. J. Biol. Chem. *275*, 30618–30622.

Yeager, T.R., Neumann, A.A., Englezou, A., Huschtscha, L.I., Noble, J.R., and Reddel, R.R. (1999). Telomerase-negative immortalized human cells contain a novel type of promyelocytic leukemia (PML) body. Cancer Res. *59*, 4175–4179.

Zhao, Q., Xie, Y., Zheng, Y., Jiang, S., Liu, W., Mu, W., Liu, Z., Zhao, Y., Xue, Y., and Ren, J. (2014). GPS-SUMO: a tool for the prediction of sumoylation sites and SUMO-interaction motifs. Nucleic Acids Res. *42*, W325–W330.

Zhu, X.-D., Küster, B., Mann, M., Petrini, J.H.J., and de Lange, T. (2000). Cell-cycle-regulated association of RAD50MRE11NBS1 with TRF2 and human telomeres. Nat. Genet. *25*, 347–352.

iScience, Volume *23*

Supplemental Information

ORCA/LRWD1 Regulates Homologous Recombination at ALT-Telomeres by Modulating Heterochromatin Organization

Rosaline Y.C. Hsu, Yo-Chuen Lin, Christophe Redon, Qinyu Sun, Deepak K. Singh, Yating Wang, Vasudha Aggarwal, Jaba Mitra, Abhijith Matur, Branden Moriarity, Taekjip Ha, Mirit I. Aladjem, Kannanganattu V. Prasanth, and Supriya G. Prasanth

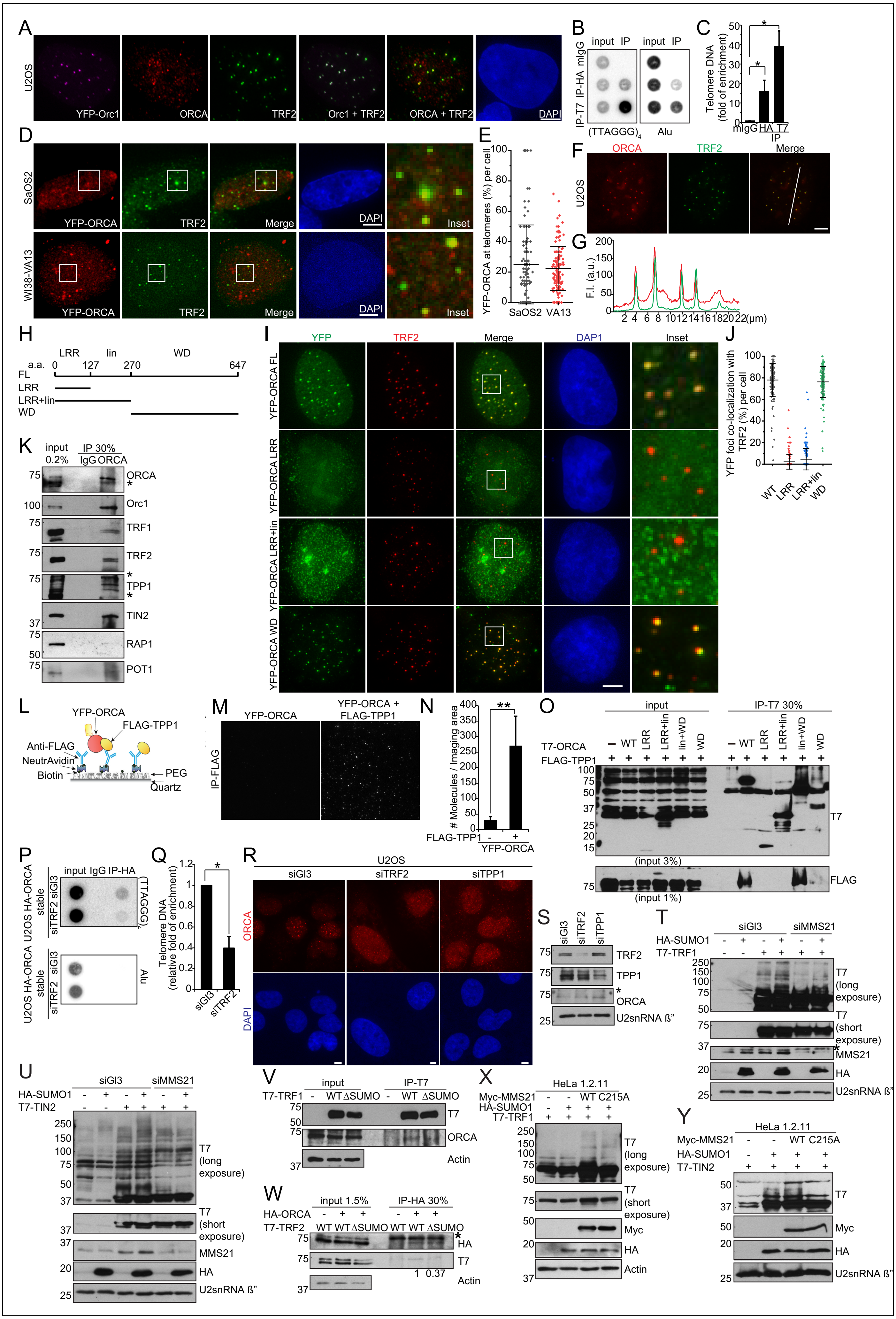
A
U2OS
YFP-Orc1
ORCA
TRF2
Orc1 + TRF2
ORCA + TRF2
DAPI
B
input IP input IP
IP-T7 IP-HA mIgG
(TTAGGG)4 Alu
C
Telomere DNA (fold of enrichment)
mIgG HA T7
IP
D
SaOS2
WI38-VA13
YFP-ORCA
TRF2
Merge
DAPI
Inset
E
YFP-ORCA at telomeres (%) per cell
SaOS2 VA13
F
ORCA TRF2 Merge
U2OS
G
F.I. (a.u.)
(μm)
H
LRR lin WD
a.a. 0 127 270 647
FL
LRR
LRR+lin
WD
I
YFP TRF2 Merge DAP1 Inset
YFP-ORCA FL
YFP-ORCA LRR
YFP-ORCA LRR+lin
YFP-ORCA WD
J
YFP foci co-localization with TRF2 (%) per cell
WT LRR LRR+lin WD
K
input 0.2%
IP 30%
IgG ORCA
ORCA
Orc1
TRF1
TRF2
TPP1
TIN2
RAP1
POT1
L
YFP-ORCA
FLAG-TPP1
Anti-FLAG
NeutrAvidin
Biotin
PEG
Quartz
M
YFP-ORCA
YFP-ORCA + FLAG-TPP1
IP-FLAG
N
Molecules / Imaging area
FLAG-TPP1 - +
YFP-ORCA
O
input
IP-T7 30%
T7-ORCA
FLAG-TPP1
WT LRR LRR+lin lin+WD WD
T7
(input 3%)
FLAG
(input 1%)
P
input IgG IP-HA
U2OS HA-ORCA stable
siGl3 siTRF2
(TTAGGG)4
Alu
Q
Telomere DNA (relative fold of enrichment)
siGl3 siTRF2
R
U2OS
siGl3 siTRF2 siTPP1
ORCA
DAPI
S
siGl3 siTRF2 siTPP1
TRF2
TPP1
ORCA
U2snRNA ß"
T
siGl3 siMMS21
HA-SUMO1
T7-TRF1
T7 (long exposure)
T7 (short exposure)
MMS21
HA
U2snRNA ß"
U
siGl3 siMMS21
HA-SUMO1
T7-TIN2
T7 (long exposure)
T7 (short exposure)
MMS21
HA
U2snRNA ß"
V
input IP-T7
T7-TRF1 - WT ΔSUMO - WT ΔSUMO
T7
ORCA
Actin
W
input 1.5% IP-HA 30%
HA-ORCA
T7-TRF2 WT WT ΔSUMO WT WT ΔSUMO
HA
T7
1 0.37
Actin
X
HeLa 1.2.11
Myc-MMS21
HA-SUMO1
T7-TRF1
WT C215A
T7 (long exposure)
T7 (short exposure)
Myc
HA
Actin
Y
HeLa 1.2.11
Myc-MMS21
HA-SUMO1
T7-TIN2
WT C215A
T7
Myc
HA
U2snRNA ß"

** p<0.01
* p<0.05

Hsu_Fig S2.

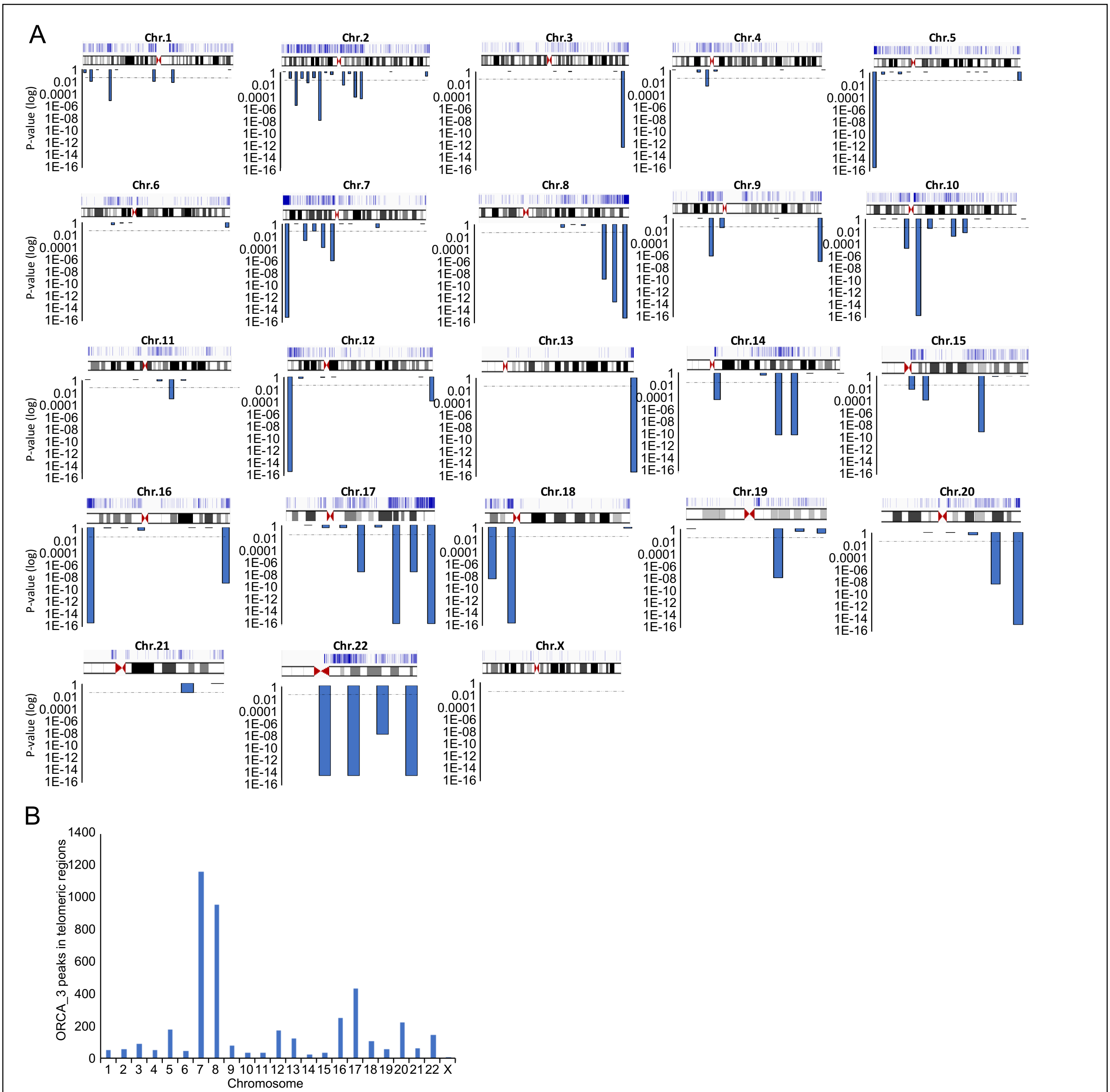
A
Chr.1
Chr.2
Chr.3
Chr.4
Chr.5
Chr.6
Chr.7
Chr.8
Chr.9
Chr.10
Chr.11
Chr.12
Chr.13
Chr.14
Chr.15
Chr.16
Chr.17
Chr.18
Chr.19
Chr.20
Chr.21
Chr.22
Chr.X
P-value (log)
1
0.01
0.0001
1E-06
1E-08
1E-10
1E-12
1E-14
1E-16
B
ORCA_3 peaks in telomeric regions
1400
1200
1000
800
600
400
200
0
1 2 3 4 5 6 7 8 9 10 11 12 13 14 15 16 17 18 19 20 21 22 X
Chromosome

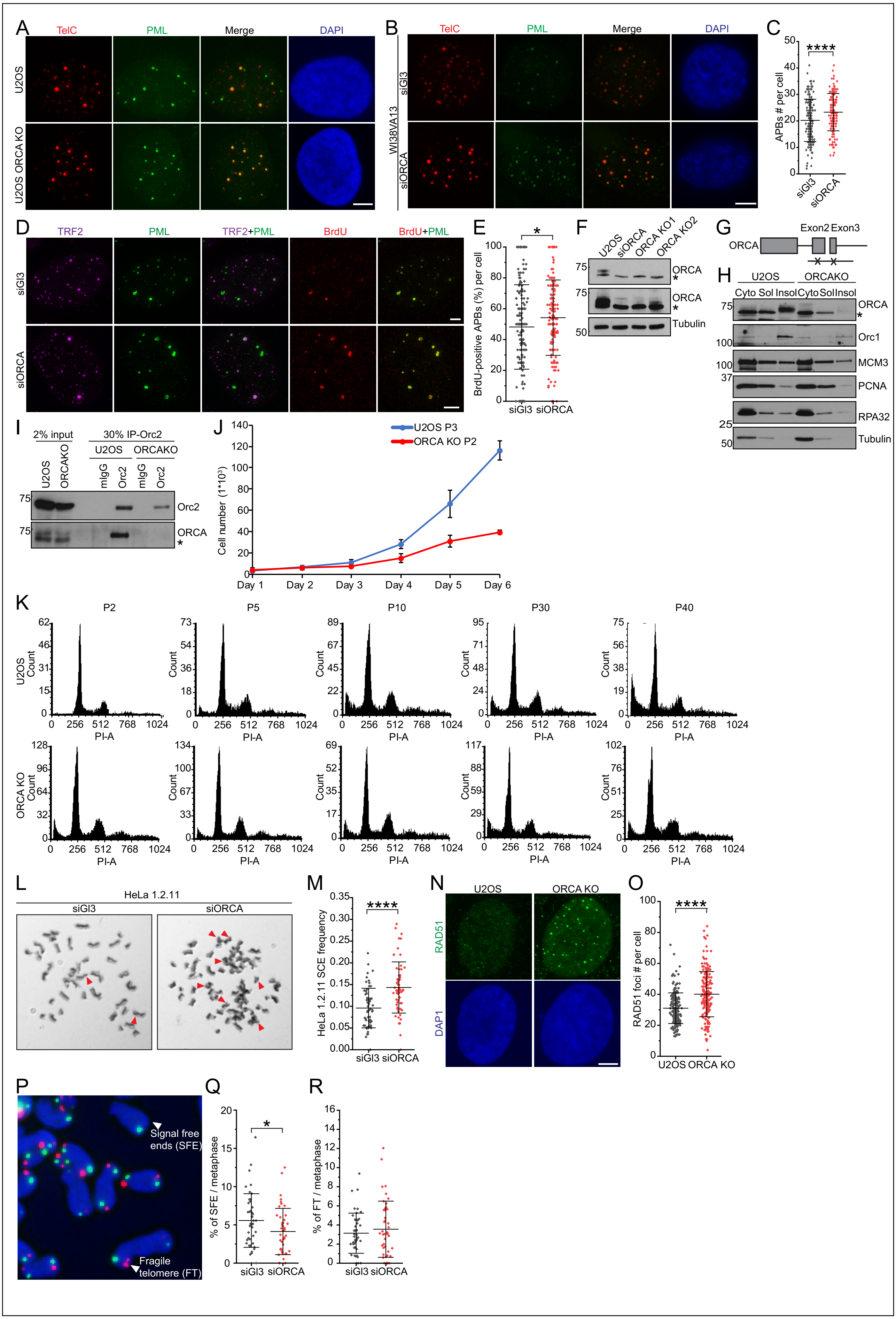

A
TelC
PML
Merge
DAPI
U2OS
U2OS ORCA KO
B
TelC
PML
Merge
DAPI
WI38VA13
siGl3
siORCA
C
APBs # per cell
****
siGl3
siORCA
D
TRF2
PML
TRF2+PML
BrdU
BrdU+PML
siGl3
siORCA
E
BrdU-positive APBs (%) per cell
*
siGl3 siORCA
F
U2OS
siORCA
ORCA KO1
ORCA KO2
ORCA
ORCA
Tubulin
G
ORCA
Exon2 Exon3
H
U2OS
ORCAKO
Cyto Sol Insol Cyto Sol Insol
ORCA
Orc1
MCM3
PCNA
RPA32
Tubulin
I
2% input
30% IP-Orc2
U2OS
ORCAKO
U2OS
ORCAKO
mIgG
Orc2
mIgG
Orc2
Orc2
ORCA
J
U2OS P3
ORCA KO P2
Cell number (1*10³)
Day 1
Day 2
Day 3
Day 4
Day 5
Day 6
K
P2
P5
P10
P30
P40
U2OS Count
ORCA KO Count
Count
PI-A
L
HeLa 1.2.11
siGl3
siORCA
M
HeLa 1.2.11 SCE frequency
****
siGl3 siORCA
N
U2OS
ORCA KO
RAD51
DAPI
O
RAD51 foci # per cell
****
U2OS ORCA KO
P
Signal free ends (SFE)
Fragile telomere (FT)
Q
% of SFE / metaphase
*
siGl3 siORCA
R
% of FT / metaphase
siGl3 siORCA

A

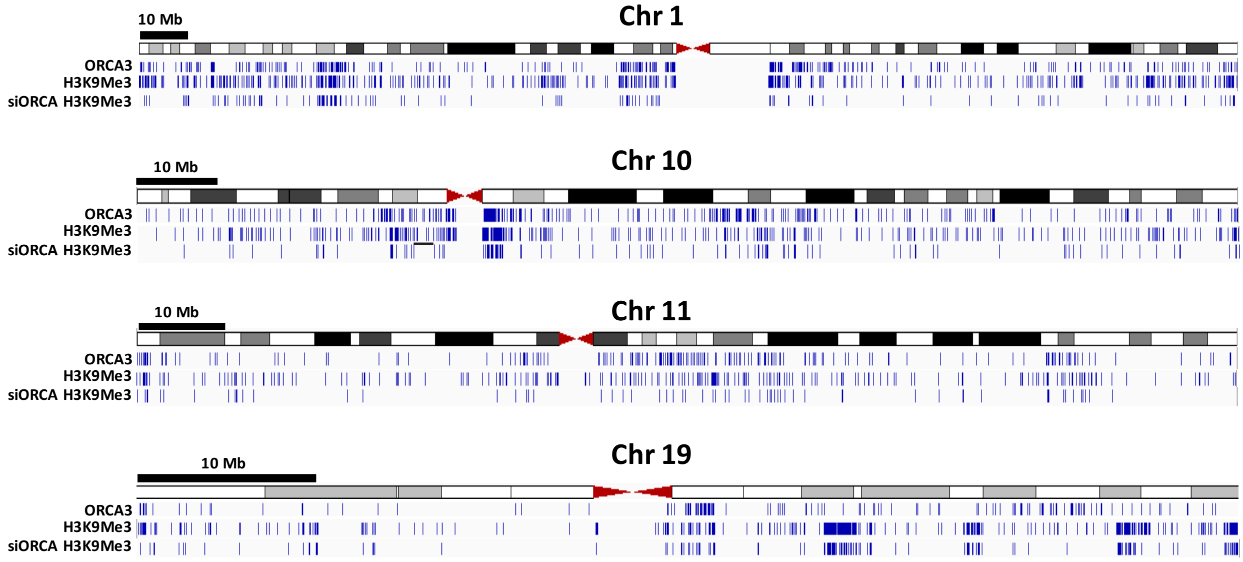

B

	H3K9me3 peaks in 10 Mb telomeric regions		H3K9me3 peaks in entire chromosmes	
	Control	siORCA	Control	siORCA
Chr7	292	198	827	314
Chr8	405	270	718	372
Chr13	73	17	106	20
Chr17	107	44	363	135
Chr20	122	60	303	139
Correlation	P=0.0002		P=0.0096	

C

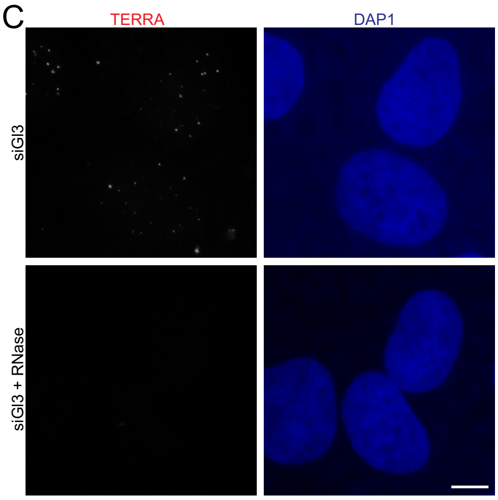

D

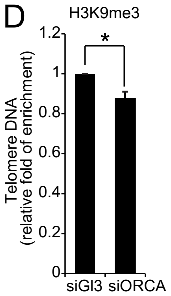

E

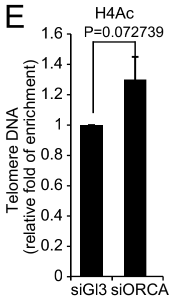

Hsu_Fig S5.

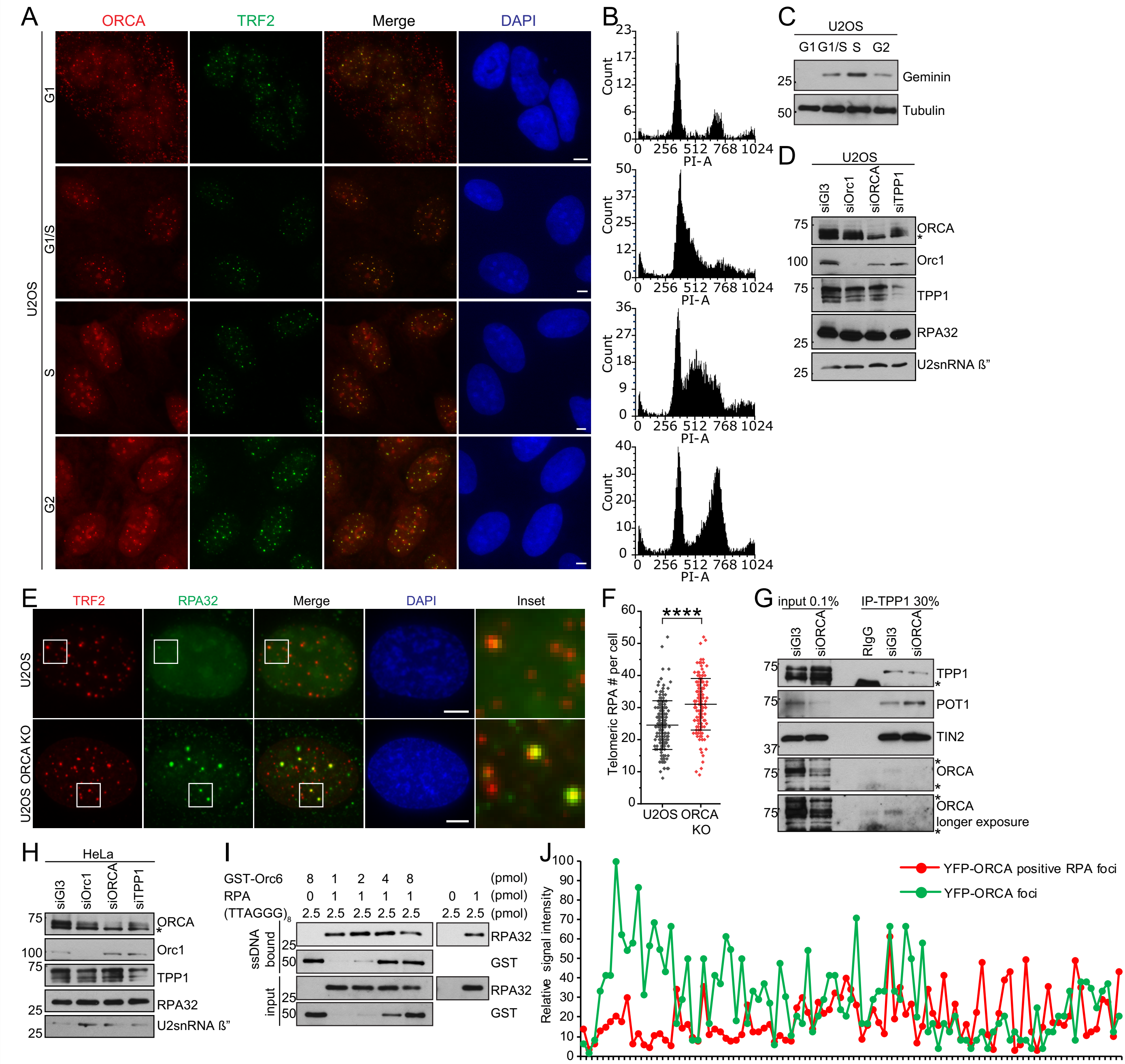
A
ORCA
TRF2
Merge
DAPI
U2OS
G1
G1/S
S
G2
B
Count
PI-A
0 256 512 768 1024
C
U2OS
G1 G1/S S G2
Geminin
Tubulin
D
U2OS
siGl3 siOrc1 siORCA siTPP1
ORCA
Orc1
TPP1
RPA32
U2snRNA ß"
E
TRF2
RPA32
Merge
DAPI
Inset
U2OS
U2OS ORCA KO
F
****
Telomeric RPA # per cell
U2OS ORCA KO
G
input 0.1%
IP-TPP1 30%
siGl3 siORCA RIgG siGl3 siORCA
TPP1
POT1
TIN2
ORCA
ORCA longer exposure
H
HeLa
siGl3 siOrc1 siORCA siTPP1
ORCA
Orc1
TPP1
RPA32
U2snRNA ß"
I
GST-Orc6 8 1 2 4 8 (pmol)
RPA 0 1 1 1 1 0 1 (pmol)
(TTAGGG)8 2.5 2.5 2.5 2.5 2.5 2.5 2.5 (pmol)
ssDNA bound
input
RPA32
GST
J
Relative signal intensity
YFP-ORCA positive RPA foci
YFP-ORCA foci

SUPPLEMENTARY INFORMATION

Figure S1. Related to Figure 1. Enrichment of ORCA at ALT-telomeres.

A Representative images of co-immunofluorescence staining of ORCA (red), telomeres (TRF2, green), and DNA (DAPI, blue) in YFP-ORC1 (pseudo-colored purple) stable U2OS cells. Scale bar denotes 5 µm.

B-C (**B**) Dot blot of HA-ORCA and T7-TRF1 TelChIP. TelChIP was conducted in U2OS HA-ORCA stable with transiently expressed T7-TRF1. (**C**). Quantification of **B**. Values (mean ± S.D.) are from three independent experiments. * $p < 0.05$

D-E (**D**) Representative images of co-immunofluorescence staining of telomeres (TRF2, green), and DNA (DAPI, blue) in SaOS2 and WI38-VA13 cells transiently expressing YFP-ORCA (red). Selected regions of merge images are shown as "Insets". Scale bar denotes 5 µm. (**E**) Quantification of YFP-ORCA co-localization with TRF2 per cell. Cell number > 120. Values (means ± S.D.) are from three independent experiments.

F-G (**F**) Co-immunolocalization of ORCA (red) and TRF2 (green) in U2OS YFP-Orc1 stable. Scale bar denotes 5 µm. (**G**) Graph shows the relative fluorescence intensity (F.I.) at the line that were scanned by confocal microscopy in **f**. a.u., arbitrary unit.

H-J (**H**) Schematic of YFP-ORCA full length and various truncated mutants. (**I**) U2OS cells transiently express YFP-ORCA full length or various truncated mutants were stained for TRF2 (red) and DNA (DAPI, blue). Selected regions of merges image are shown as "Insets". Scale bar denotes 5 µm. (**J**) Quantification of YFP foci (in **I**) co-localization with TRF2 per cell. Cell number > 150. Values (means ± S.D.) are from three independent experiments.

K Immunoprecipitation (IP) of endogenous ORCA in U2OS cells, and the protein complex was analyzed by Western blotting. ORC1 serves as the positive control. '*' denotes cross-reacting bands.

L-N (**L**) Schematic of Single Molecule Pulldown (SiMPull) assay for ORCA-TPP1 interaction. (**M**) Total internal reflecting fluorescence (TIRF) images of YFP-molecules pulled down from U2OS cell lysates expressing YFP-ORCA and FLAG-TPP1 using biotinylated FLAG antibody. YFP-ORCA alone was used as the negative control. (**N**) Average number of YFP fluorescent molecules per imaging area (5,000 μm^2). Values (means ± S.D.) are from three independent experiments. **, $P < 0.01$.

O Co-IP of various T7-ORCA truncated mutants with FLAG-TPP1, the protein complex was analyzed by Western blotting. '*' denotes cross-reacting band.

P-Q (**P**) Dot blot of HA-ORCA TelChIP in control or TRF2-depleted sample. (**Q**). Quantification of **P**. Values (mean ± S.D.) are from three independent experiments. * $p < 0.05$

R-S (**R**) Representative images of ORCA (red) in U2OS YFP-Orc1 stable cell line upon shelterin components depletion. Cells were stained with ORCA and DNA (DAPI, blude). Scale bar denotes 5 µm. (**S**) Whole cell lysate of (**R**) was analyzed by Western blotting. U2snRNAß" is used as loading control. '*' denotes cross reacting band.

T. The SUMOylation level of T7-TRF1 in U2OS treated with control or siMMS21 was analyzed with Western blotting. * denotes cross-reacting bands.

U. The SUMOylation level of T7-TIN2 in U2OS treated with control or siMMS21 was analyzed with Western blotting.

V. Immunoprecipitation of T7-TRF1 WT or SUMO-deficient (ΔSUMO) mutant in U2OS expressing HA-ORCA. The protein complex was analyzed by Western blotting.

W. Immunoprecipitation of HA-ORCA in U2OS expressing T7-TRF2 WT or SUMO-deficient (ΔSUMO) mutant. The protein complex was analyzed by Western blotting. * denotes cross-reacting bands.

X. The SUMOylation level of T7-TRF1 in HeLa 1.2.11 transiently expressing Myc-MMS21 WT or C215A was analyzed with Western blotting.

Y. The SUMOylation level of T7-TIN2 in HeLa 1.2.11 transiently expressing Myc-MMS21 WT or C215A was analyzed with Western blotting.

Figure S2. Related to Figure 2. Enrichment of ORCA at select subtelomeres

A Graphs showing the p-values (logarithmic scale) for Poisson tests comparing peak density in 10 Mb regions alongside each chromosome (bars) with the average density per 10 Mb for all chromosomes. Images above the graphs are composites from IGV screenshots with chromosomes in black and ORCA peak density in blue. For convenience, p-values < 2.2E-16 are shown as 2.2E-16. The dashed lines designate p-values of 0.05. Poisson tests were performed with RStudio using a level of confidence of 0.95 and the alternative "greater". This figure is related to Fig. 2B.

B Quantification of ORCA peaks from mid G1 (ORCA_3, 3hrs into G1) located within 10 Mb of p and q telomeric regions from U2OS cells' chromosomes.

Figure S3. Related to Figure 3. ORCA regulates ALT activity.

A Representative images of G2 enriched U2OS WT and ORCA KO cells stained with PML (green) and Telomere DNA (TelC, red). Scale bar denotes 5 µm.

B-C (**B**) Representative images of G2 enriched WI38-VA13 cells treated with control or siORCA. Cells were stained with PML (green) and Telomere DNA (TelC, red). Scale bar denotes 5 µm. (**C**)

Quantification of **B**. APB bodies are defined as the co-localization of PML and TelC. The number of APBs per cell were measured. Cell number > 160. Values (means ± S.D.) are from three independent experiments. ****, P< 0.001.

D-E (**D**) Representative images of G2 enriched (as shown in schematic) U2OS cells treated with control or siORCA, labeled with BrdU (100 μM) for 3 h. Cells were stained with TRF2 (Cy5), PML (green), BrdU (red), and DNA (DAPI, blue). Scale bar denotes 5 μm. (**E**) Quantification of percentages of BrdU-positive APBs percell were measured. Cell number > 160. Values (means ± S.D.) are from three independent experiments. Note the ring-shaped distribution of PML as captured by high-resolution imaging, consistent with EM studies. *, P < 0.05.

F U2OS ORCA KO cells were validated by Western blotting.

G Schematic of sgRNA design for generating ORCA KO cell lines.

H Chromatin fractionation in U2OS WT and ORCA KO cells.

I IP of ORC2 in U2OS WT or ORCA KO cells, the protein complex were analyzed by Western blotting. '*' denotes cross-reacting band.

J Cell proliferation assay of U2OS WT and ORCA KO.

K PI flow analysis of different passages of U2OS WT and ORCA KO cells.

L-M (**L**) Representative images of harlequin chromosomes in HeLa 1.2.11 cells treated with control or siORCA. Arrowheads indicate chromosomes with Sister Chromatid Exchange. Scale bar denotes 5 μm. (**M**) Sister Chromatid Exchange (SCE) frequency (number of exchanges per metaphase spread) was measured in HeLa 1.2.11 cells treated with control or siORCA (Metaphase spread N > 60). Values (means ± S.D.) are from three independent experiments. ****, P< 0.001

N-O (**N**) Representative images of G2 enriched U2OS WT and ORCA KO cells stained with RAD51 (green) and DNA (DAPI, blue). Scale bar denotes 5 μm. (**O**) The number of RAD51 foci per cell were measured. Cell number > 190. ****, P< 0.001.

P-R (**P**) Representative image of Chromosome orientation FISH (CO-FISH) using TelC (red) and TelG (green) probes in U2OS cells showing Signal Free Ends (SFE) and Fragile Telomeres (FT). (**Q**) The percentages of SFE and (**R**) FT per metaphase spread in control and siORCA-treated U2OS cells were measured (metaphase spread N > 40). Values (means ± S.D.) are from three independent experiments. *, P < 0.05.

Figure S4. Related to Figure 4. Telomere heterochromatin status in the absence of ORCA.

A Composite images from IGV screenshots showing ORCA and H3K9me3 peak densities (blue) in 4 chromosomes (1, 10, 11 and 19) that are not enriched for ORCA peaks at the sub-telomere regions. H3K9me3 peaks in the absence of ORCA are also shown.

B H3K9Me3 peak distributions in chromosomes 7, 8, 13, 17 and 20. Number of peaks located in the 10 Mb telomeric regions (p arm of Chr 7 and q arms of Chr 8, 13, 17 and 20, left) as well as peaks located in the entire chromosomes (right) in control and siORCA-treated U2OS cells are shown. P values from Pearson correlations for H3K9Me3 peaks between control and siORCA-treated cells in the 10 Mb telomeric regions (p=0.0002) and in entire chromosomes (p=0.0096) are also shown. Pearson correlations were calculated using GraphPad Prism. The table is related to Fig. 4A.

C Representative images of TERRA RNA FISH signal in control and RNase treated cells. Scale bar denotes 5 μm.

D-E (**D**) Quantification of H3K9me3 TelChIP in control or siORCA treated sample. Values (mean ± S.D.) are from three independent experiments. *, $P < 0.05$. (**E**) Quantification of H4Ac TelChIP in control or siORCA treated sample. Values (mean ± S.D.) are from three independent experiments.

Figure S5. Related to Figure 5. ORCA localization at telomeres during the cell cycle

A-C (**A**) U2OS YFP-ORC1 stable cells were synchronized at different stages of the cell cycle, and stained with ORCA (red), TRF2(green), and DNA (DAPI, blue). Scale bar denotes 5 µm. (**B**) Cells synchronized during different stages of the cell cycle as shown in **A** by PI flow analysis. (**C**) Samples in **A** were analyzed by Western blotting. Geminin was used as marker to show the synchronization.

D The knockdown efficiency of siORC1, siORCA, and siTPP1 in U2OS cells was analyzed by Western blotting. '*' denotes cross-reacting band.

E-F (**E**) Representative images of G2 enriched U2OS WT and ORCA KO cells stained with TRF2 (red), RPA32 (green), and DNA (DAPI, blue). Selected regions of merged images are shown as "Insets". Scale bar denotes 5 µm. (**F**) The number of telomeric RPA foci per cell were measured. Cell number > 160. Values (means ± S.D.) are from three independent experiments. ****, $P < 0.001$.

G Immunoprecipitation using TPP1 antibody in control and ORCA-depleted U2OS cells and analyzed by immunoblotting. '*' denotes cross-reacting band.

H The knockdown efficiency of siORC1, siORCA, and siTPP1 in HeLa cells was analyzed by Western blotting. '*' denotes cross-reacting band.

I Biotinylated $(TTAGGG)_8$ pulldown assay using purified ORC6 and RPA. The amount of ssDNA-binding proteins was analyzed using Western blotting.

J Upon co-localization, the correlation of ORCA signal intensity and RPA32 signal intensity of 100 foci was measured.

Transparent Methods

KEY RESOURCES TABLE

REAGENT or RESOURCE	SOURCE	IDENTIFIER
Antibodies		
TRF1	Santa Cruz	sc-56807
TRF2	Millipore	4A794
TPP1	Santa Cruz	sc-100597
POT1	Millipore	EPR6319
TIN2	Dr. Titia de Lange, Rockefeller University	#864
RAP1	Dr. Titia de Lange, Rockefeller University	#765
Flag	Sigma	M2
HA		12CA5
T7	Novagen	69522
ORCA pAb	(Shen et al., 2010)	2854-1 (IP; IF); 2853-2 (IB)
ORC1 pAb	Self-made	2518-2
ORC2 pAb	Self-made	205-6
Geminin	Santa Cruz	sc-13015
MCM3		pAb738

α-tubulin	Sigma	T5168
PCNA	Santa Cruz	PC10
γH2AX	Abcam	ab2893
RPA70	Bethyl Laboratories	A300-241A
RPA32	Santa Cruz	sc-56770 (IB)
GST	Santa Cruz	sc-138
RAD51	Santa Cruz	sc-8349
RPA32	Cell Signaling	4E4 (IF)
TRF2	Novus	NB110-57130
PML	Santa Cruz	sc-966
BrdU	BD	347580
Chemicals, Peptides, and Recombinant Proteins		
RO-3306 (CDK1 inhibitor)	Sigma	SML0569
Thymidine	Sigma	T9250-10G
mPEG/biotin-PEG	Laysan Bio, Inc, Arab, AL	MPEG-SC-5000/Biotin-PEG-SC-5000
Neutravidin	Pierce, Rockford, IL	31000
BSA	Sigma	A9418
Micrococcal nuclease (MNase)	Sigma	N3755
GammaBind G Sepharose	GE Healthcare	17-0885-02
BrdU	Sigma	B5002-250MG
BrdC	hem-Impex Internation	00402
Etoposide	Sigma	E1383

TelC-TMR (TMR-OO-CCCTAACCCTAACCCTAA)	Panagene	F2001
TelG-FITC (FITC-OO-KKK-TTAGGGTTAGGGTT	Panagene	F1010
streptavidin-magnetic beads	ThermoFisher Scientific	65002
Oligonucleotides		
biotinylated $(TTAGGG)_8$	5'-$(TTAGGG)_8$-biotin-3'	
c-circle probe	5'-CTAACCCTAACCCTAACC-3'	
Recombinant DNA		
Orc1 and ORCA constructs	(Shen et al., 2010)	
pCDNA-3xFLAG-NLS-TPP1	Dr. Steven Artandi	Addgene plasmid # 53585
hRPA and YFP-RPA2	Dr. Marc Wold (University of Iowa)	
CFP-TRF1 and pLPC-Myc-TRF2	Dr. Titia de Lange (Rockefeller University)	
Myc-MMS21 WT and C215A	Dr. Patrick Ryan Potts (St. Jude Children's Researh Hospital)	
Software and Algorithms		
ImageJ	NIH	
Axiovision software	Zeiss	

CONTACT FOR REAGENT AND RESOURCE SHARING

Further information and requests for resources and reagents should be directed to and will be fulfilled by the Lead Contact, Dr. Supriya Prasanth (supriyap@illinois.edu, Department of Cell and Developmental Biology, University of Illinois at Urbana-Champaign, 601S Goodwin Avenue, Urbana, IL 61801 USA).

EXPERIMENTAL MODEL AND SUBJECT DETAILS

Cell culture

U2OS, WI38-VA13, and HeLa 1.2.11 cells (a generous gift from Dr. Rachel Flynn, Boston University School of Medicine) cells were grown in Dulbecco's modified Eagle's medium (DMEM) containing high glucose and supplemented with 5% fetal bovine serum (FBS—HyClone GE, Pittsburg, PA). SaOS2 was grown in Macoy's 5A medium containing supplemented with 15% fetal bovine serum. U2OS YFP-ORC1 and HA-ORCA stable cell line were generated as previously described (Shen et al. 2010).
For transient transfection, cells were transfected with Lipofectamine 2000 (Invitrogen) as per the manufacturers' protocol.

CRISPR-Cas9 design and analysis
The plasmids for generating ORCA KO in U2OS cell line were obtained from Dr. David A. Largaespada (University of Minnesota). The sgRNA were designed using the website (http://zifit.partners.org/ZiFiT/references.aspx). The target regions were indicated in Figure S3G. To generate KO cells, U2OS were co-transfected with plasmids containing the targeting sequences and selected for single cell colonies. These colonies were analyzed by Western blotting with ORCA antibodies.

sgRNA targeted ORCA sequence: GCCATTGACCTTACGGAGCG
sgRNA targeted ORCA sequence: GTGAACTCGCTGAGGGACTC

METHOD DETAILS

Cell synchronization
For endogenous ORCA IP at different stages of the cell cycle, U2OS cells were synchronized either by double thymidine block and release or nocodazole block and release. For G1/S, S, and G2 phase, cells were grown in the presence of 2 mM thymidine for 24 h. After the first block, thymidine was removed by repeatedly washing the cells in PBS and cells were released for 12 h in fresh medium. Finally, cells were synchronized at G1/S by further growing them in the presence of 2 mM thymidine for 24 h. The cells were released in fresh medium for 4 h to collect them in S phase; and 8 h for G2 phase. For M phase, cells were synchronized at prometaphase by treating them with 50 ng/ml nocodazole for 12–16 h. For G1 phase, after nocodazole treatment, shake-off cells were washed three times with PBS and releasing them in the fresh medium for 3 h. Synchronized samples were evaluated by flow cytometry.
For G2 enrichment, cells were first blocked with 2 mM thymidine for 16h, then released in RO-3306 (CDK1 inhibitor, 10 μM) containing medium for 20h.

siRNA
For siRNA transfection, cells were grown to 30% confluency and siRNA against target or control luciferase gene (Shen et al., 2010) was delivered into the cells at a final concentration of 100 nM using Lipofectamine RNAimax (Invitrogen, Carlsbad, CA). The siRNAs were delivered twice at the gap of 24 hr, and the cells were collected 48 hr after the second round of transfection for subsequent analysis.

siRNA sequence:
siORCA: 5'-CCAACCAGGACUACGAAUU-3'
siORC1: 5'-CUGCACUACCAAACCUAUA-3'
siTRF2: 5'-AAGAGGCAGUCAAUCGCUGG-3'G
siTPP1: 5'-GACUUAGAUGUUCAGAAAA-3'
siMMS21: 5'- CUCUGGUAUGGACACAGCU-3'

Single Molecule Pulldown (SiMPull)

SiMPull experiments were carried out in flow chambers prepared on quartz microscope slides, which were passivated with methoxy-polyethylene glycol (mPEG) doped with 1% biotin-PEG (Jain et al., 2011). Appropriate biotinylated antibody was immobilized on PEG passivated surfaces at approximately 20 nM concentration for 20 min after coating the flow chambers with 0.2 mg/ml NeutrAvidin for 5 min. Cells were collected 24 h after transient transfection, and lysed in high salt buffer (50 mM Tris-HCl pH 7.4, 500 mM NaCl, 10% glycerol, 0.25% Triton X-100 with protease inhibitors) at 4°C for 20 min. Equal amount of zero salt buffer were added and incubated for another 10 min. After centrifugation, the supernatants were used for SiMPull analysis. Samples were appropriately diluted with T50 buffer (10 mM Tris-HCl pH 8.0, 50 mM NaCl 0.1 mg/ml BSA) to obtain optimal single molecule density on the surface. Diluted Samples were incubated in the chamber for 20 min and washed with the buffer. Single-molecule data were acquired by a prism-type TIRF microscope and analyzed using scripts written in Matlab.

SiMPull data analysis

Single molecule data were acquired as the average number of YFP fluorescent molecules per imaging area (5,000 μm^2) as shown in the histograms. The error bars represent standard deviation of the mean values from 30 imaging areas.

Immunoprecipitation and immunoblots

For endogenous ORCA immunoprecipitation, the U2OS cells were lysed in IP buffer (50 mM HEPES pH 7.9, 350 mM NaCl, 10% Glycerol, 0.1% Triton X-100, 1 mM $CaCl_2$ with protease and phosphatase inhibitors) at 4°C for 20 min. Micrococcal nuclease (MNase, N3755, Sigma-Aldrich) was added to a final concentration of 0.03 U/µl, and incubated at room temperature (RT) for 20 min. After pre-clearing with Gammabind Sepharose beads for 30 min, the lysates were incubated with appropriate antibody overnight. After pulled down the beads were washed with IP buffer and finally denatured by the addition of Laemmli buffer.

For endogenous TPP1 and ORC2 immunoprecipitation, the cells were first lysed in IP buffer (50 mM Tris-HCl pH 7.4, 500 mM NaCl, 10% glycerol, 0.25% Triton X-100 with protease and phosphatase inhibitors) at 4°C for 20 min, and equal volume of zero salt buffer was added. After centrifugation, the supernatant was pre-cleared, incubated with appropriate antibody overnight, pulled down and washed with wash buffer (50 mM Tris-HCl pH 7.4, 250 mM NaCl, 10% glycerol, 0.25% Triton X-100 with protease and phosphatase inhibitors).

For co-IP, 24 h after transient transfection, U2OS cells were lysed in IP buffer (50 mM Tris-HCl pH 7.4, 500 mM NaCl, 10% glycerol, 0.25% Triton X-100 with protease and phosphatase inhibitors) at 4°C for 20 min, and equal volume of zero salt buffer was added. After centrifugation, the supernatant was precleared, incubated with appropriate antibody overnight, pulled down and washed with IP buffer. The IP result was analyzed by Western blotting.

Immunoflourescence staining, Immuno-Fluorescence In Situ Hybridization (Immuno-FISH), Chromosome Orientation FISH (CO-FISH), and RNA FISH

For Immunofluorescence staining, cells were pre-extracted with 0.3% Triton X-100 in Cytoskeletal buffer (CSK: 100 mM NaCl, 300 mM Sucrose, 3 mM MgCl2, 10 mM PIPES pH 6.8) for 3 min on ice followed by fixation with 2% paraformaldehyde in phosphate buffered saline (PBS, pH 7.4) for 15 min in RT. For HeLa 1.2.11 cell, cells were permeabilized with 0.1% Triton X-100 in CSK at room temperature (RT) for 5 min after fixation. Blocking was then done for 30 min with 1% Normal goat serum (NGS) in PBS. Primary antibody incubation was then carried out for 1 or 2 h in a humidified chamber followed by secondary antibody incubation for 1 h at RT. The cells were then stained with DAPI (4',6-Diamidino-2-Phenylindole) and mounted using VECTASHIELD (Vector Laboratories Inc., Burlingame, CA).

For BrdU incorporation at APB bodies, cells were labeled with 100 μM for 2h or 3h before fixation.

For immuno-FISH, after secondary antibody staining, the cells were washed and fixed with 4% paraformaldehyde for 15 min at RT. Cells were then dehydrated in successive chilled ethanol (70%, 95%, 100%), and the coverslips were dried. TelC-TMR probe was diluted in hybridization buffer (70 % formamide, 10 mM NaHPO4 pH 7.5, 10 mM NaCl, 20 mM Tris-HCl pH 7.5) and added to coverslips. After denaturation at 80°C for 5 min, the coverslips were incubated at RT for 2 h. The coverslips were washed in buffer 1 (1XPBS with 0.1% Tween 20) at 57°C for 20 min, and buffer 2 (2X SSC with 0.1% Tween 20) at RT for 1 min. The coverslips were stained with DAPI at RT FOR 20 min, washed with buffer 2, and mounted using VECTASHIELD.

For CO-FISH, cells were treated with 2 mM thymidine for 20 h, and released in BrdU/BrdC (30 μM/ 10 μM) for 20 h. The metaphase spread was prepared by incubating cells with nocodazole for 4 h, collected by shake-off, and incubated in 75 mM KCl at 37°C for 40 min. Cells were fixed in chilled fixative (3:1 ethanol/acetic acid) before dropping on glass slides. Metaphase spread was rehydrated in PBS, fixed with 3.7% formaldehyde in PBS for 4 min, washed with PBS, and incubated with 0.5 μg/ml H33258 (Sigma, B2883) at RT for 15 min. The sample was then exposed to UV ($5.4X10^3$ J/m^2), and digested with ExoIII (6U/μl) at 37°C for 30 min. After wash, the sample was dehydrated in successive chilled ethanol (70%, 95%, 100%), dried, and incubated with TelC-TMR probe diluted in hybridization buffer. The sample was denaturation at 80°C for 5 min, and incubated at RT for 2 h. After incubation, the sample was washed with buffer 1 (70% formamide, 20 mM Tris-HCl pH 7.4) and buffer 2 (50 mM Tris-HCl pH 7.4, 150 mM NaCl, 0.05% Tween 20). The sample was incubated with TelG-FITC (FITC-OO-KKK-TTAGGGTTAGGGTT, Panagene) for another 2 h at RT, washed with buffer 3 (2XSSC with 50% formamide), buffer 2, and dehydrated again with successive chilled ethanol. After dried, the cells were mounted using VECTASHIELD.

For TERRA RNA FISH, cells were pre-extracted with 0.1% Triton X-100 on ice for 3 min, fixed in 4% paraformaldehyde, permeabilized with 0.5% NP40 in PBS at RT for 10 min, and blocked with 0.5% BSA in PBS for 1 h at RT. For RNase treatment, the cells were incubated with 200 μg/ml RNase A at 37°C for 30 min after blocking. 10 nM of TelC-TMR probe was diluted in hybridization buffer (50% formamide, 10 mM ribonucleoside vanadyl complex, 2X SSC, 2 mg/ml BSA, 10% dextran sulphate). The cells were incubated with probes in a humidified chamber at 39°C for 18 h. The cells were washed with 2XSSC in 50% formamide at 39°C, 2XSSC at 39°C, and 2XSSC at RT. After wash the cells were stained with DAPI, and mounted with VECTASHIELD.

Zeiss Axioimager z1 fluorescence microscope (Carl Zeiss Inc., Jena, Germany) equipped with chroma filters (Chroma technology, Bellows Falls, CA) was used for observing the cells and statistics. Axiovision software (Zeiss) was used for digital imaging using Hamamatsu ORCA cooled CCD camera. Cells were also examined on the Delta vision optical sectioning deconvolution instrument (Applied precision, Pittsburgh, PA) on an Olympus microscope.

C-circle assay

C-circle assay was performed as described (Henson et al., 2017). The genomic DNA was purified using the Quick C-Circle Preparation (QCP) method. The DNA samples were diluted with 1X QCP buffer. 40 ng of DNA (10 µl) was combined with 10 µl Master mix containing 7.56 mM DTT, 2X Φ29 NEB buffer, 8 µg/ml BSA, 0.2% Tween-20, 2 mM each dATP, dGTP, dTTP, dCTP with or without 7.5 U Φ29 DNA polymerase. Samples were incubated at 30°C for 8 h, and then at 65°C for 20 min. The reaction products were mixed with 40 µl 2XSSC and dot-blotted onto a nylon memberane. After UV cross-link, the membrane was hybridized with P^{32} labeled probe (5'-CTAACCCTAACCCTAACC-3'). After wash the blots were exposed to Phosphorimager and quantified with ImageJ. The same blot was stripped with 0.1% SDS 0.5X SSC at 65°C until the c-circle signal is gone, then probed with Alu probe (5'-CGGAGTCTCGCTCTGTCGCCCAGGCTGGAGTGCAGTGGCGCGA-3') for loading control.

Sister Chromatid Exchange (SCE)

For sister chromatid exchange, after two rounds of knockdown, U2OS cells were labeled with two rounds of 20 µM BrdU (100 µM BrdU for HeLa 1.2.11). Etoposide (5 µM) was added with second round of BrdU for 4 h, washed off for 4 h, and nocodazole was added for making metaphase spread. The metaphase spread sample was first immerse in 10 µg/ml H33258 for 20 min at RT, and rinsed with sorenson's buffer. The sample was exposed to UV for 30 min, and incubated in 1X SSC at 50°C for 1 h. The sample was stained with Giemsa statin (ACROS Organics), and mount with Quick-hardening mounting medium (Sigma, 03989). SCE frequency was calculated as number of exchange / chromosome number of metaphase spread.

TERRA RT-qPCR

TERRA RT-qPCR were performed as described previously with slight modifications and primers were from these previous studies too (Arnoult et al., 2012; Feretzaki and Lingner, 2017; Porro et al., 2010; Scheibe et al., 2013). Briefly, RNA was purified with RNeasy Mini Kit (Qiagen #74104) with DNase treatment (RNase-Free DNase Set (Qiagen, #79254) as per manufacturer's instruction. Reverse transcription was performed using SuperScript III Reverse

Transcriptase (Invitrogen, 18080044) with gene specific primers (shown in primer table). Terra levels were measured by Real-time RT-PCR using the SYBR Green I fluorogenic dye on StepOne plus system (Applied Biosystems). Primer sets used for RT-qPCR are listed in the primer table below and normalized against beta actin levels.

Protein Purification

The purification of RPA was described previously (Leigh A. Henricksen, 1994). For purification of GST-ORCA, vectors containing bacterially expressed GST-ORCA or GST were transformed into *E.coli* BL21. Overnight culture was diluted 1:200 into 200ml of LB medium and cultured at 37°C until OD reached 0.6. Cultures were then induced with 1 mM IPTG and grown at 18°C with shaking overnight. The pelleted bacterial culture was resuspended with lysis buffer (50 mM Tris-HCl pH 7.5; 0.1 mM EDTA; 150 mM NaCl; 1 mM DTT, 0.1% Triton X-100; 5% glycerol) supplemented with protease inhibitor and 0.5 mg/ml lysozyme (Sigma) and incubated on ice for 45min. The lysate was then sonicated and pelleted by centrifugation and the supernatant was incubated with 1ml of Glutathione-resin (Sigma, G4510) for 30 min at 4°C. Beads were washed three times with wash buffer (50 mM Tris-HCl pH7.5; 500 mM NaCl; 0.1 mM EDTA; 1 mM DTT; 5% glycerol) at 4°C. GST-tagged proteins were finally eluted with 1 ml elution buffer (50 mM Tris-HCl pH7.5; 500 mM NaCl; 0.1 mM EDTA; 1 mM DTT; 5% glycerol 20 mM reduced glutathione).

ORCA-RPA Direct interaction

Purified RPA (360 ng) and GST-ORCA (500 ng) was incubated in binding buffer (1X PBS 0.02% NP40 with protease inhibitors) at 4°C for 30 min, and incubated with RIgG or anti-ORCA pAb (2854-1 AP) at 4°C for 1 h. The protein-antibody mixture was pulled down with Gammabind Sepharose beads at 4°C for 1 h, washed with binding buffer, and analyzed with Western blotting.

ORCA-RPA ssDNA binding assay

The ORCA-RPA ssDNA binding assay was modified from (Flynn et al., 2011). Briefly, 2.5 pmol of biotinylated $(TTAGGG)_8$ were attached to streptavidin-magnetic beads (ThermoFisher Scientific, 65002) in DNA binding buffer (10 mM Tris-HCl pH 8.0, 100 mM NaCl) at RT for 30 min. Purified RPA (1 pmol) was incubated with different amount of GST-ORCA or ORC6 in protein binding buffer (10 mM Tris-HCl pH 7.5, 100 mM NaCl, 10% glycerol, 0.02% NP-40, 100 μg/ml BSA) at 4°C for 30 min. The protein mixture was incubated with ssDNA-beads in protein binding buffer at RT for 30 min. The protein-DNA complex was washed 3 times with protein binding buffer, and the ssDNA-bound fraction was analyzed by Western blotting.

Telomere Chromatin Immunoprecipitation (TelChIP)

Cells were fixed with 1% formaldehyde, quenched with 0.125 M glycine, and pelleted in PBS. Pellets were lysed in solution A (10 mM HEPES pH 7.9, 1 mM EDTA, 0.5 mM EGTA, 0.25% Triton X-100). Nuclear pellets were isolated by centrifugation and lysed in solution B (10 mM HEPES pH 7.9, 1 mM EDTA, 0.5 mM EGTA, 200 mM NaCl). After centrifugation the pellets were lysed in solution C (50 mM HEPES pH 7.9, 0.1% Sodium deoxycholate, 150 mM NaCl, 0.1% SDS, 1% Triton X-100) and sonicated. After centrifugation the chromatin was pre-cleared with magnetic beads. Pre-cleared chromatin was incubated with indicated antibodies overnight, pulled down with magnetic beads, and washed with buffer 1 (50 mM HEPES pH 7.9, 0.1% Sodium deoxycholate, 2 mM EDTA, 150 mM NaCl, 1% Triton X-100), buffer 2 (50 mM HEPES pH 7.9, 0.1% Sodium deoxycholate, 2 mM EDTA, 500 mM NaCl, 1% Triton X-100), buffer 3 (10 mM Tris-HCl pH 8.0, 0.5% Sodium deoxycholate, 1 mM EDTA ,250 mM LiCl, 0.5% NP-40), and TE/DTT buffer (10 mM Tris-HCl pH 8.0, 1 mM EDTA, 1 mM DTT). DNA was eluted in elution buffer (0.1 M $NaHCO_3$, 0.5% SDS), and the level of pulled down DNA was analyzed by dot blot using telomere specific probe $(TTAGGG)_4$. The signal was detected with a Phosphor Imager screen and quantified using ImageJ (https://imagej.nih.gov/ij/). For calculating the fold of enrichment, the level of pulled down telomeric DNA was normalized to that of control IgG. For calculating the relative fold of enrichment, the pulled down telomeric DNA in knockdown sample was normalized to that of control (siGl3). Alu probe (CGGAGTCTCGCTCTGTCGCCCAGGCTGGAGTGCAGTGGCGCGA) was used as loading control. The following antibodies were used for TelChIP: anti-T7 (Novagen, Billerica, MA), anti-HA 12CA5, anti-H3K9me3 (Diagenode, NJ, USA), and anti-acetyl-Histone H4 (06-598, Millipore, MA, USA).

Flow cytometry

For flow cytometry, cells were fixed in chilled ethanol overnight after resuspention in PBS with 1% NGS. After two rounds of washing, cells were resuspended in PBS with 1% NGS with 120 mg/ml propidium iodide and 10 mg/ml RNase A followed by 30 min incubation at 37°C. DNA content was measured by BD FACS Canto II and analyzed with FCS Express 5. For ORCA KO cell validation, at least 2,500 cells were collected for analysis. For other experiments, at least 5,000 cells were collected for analysis.

Chromatin fractionation

Detailed procedure was described previously(Shen et al., 2010). To isolate chromatin, cells were resuspended in buffer A (10 mM HEPES pH 7.9, 10 mM KCl, 1.5 mM $MgCl_2$, 0.34 M sucrose, 10% glycerol, 1 mM DTT, 0.1% Triton X-100 with protease inhibitors) for 5 min on ice. The cytoplasmic fraction (Cyto) was separated by centrifugation (1,400g, 4 min). The isolated nuclei were lysed in buffer B (3 mM EDTA, 0.2 mM EGTA, 1 mM DTT with protease inhibitors) for 30 min on ice. The nuclear soluble fraction (Sol) was collected by centrifugation (1,700g 4 min). Finally the chromatin insoluble fraction (Insol) was resuspended in buffer A (without Triton X-100) and sonicated. All the fractions were mixed with Laemmli buffer, denatured, and analyzed by Western blotting.

Genome-wide distribution of ORCA and H3K9Me3

Files for ORCA and H3K9Me3 peaks (33) located within 10 Mb of p and q telomeric regions were generated using the export features from the Integrative Genomics Viewer (IGV). Analysis for peak distribution and peak density across chromosomes were performed using Excel with x- and y-coordinates corresponding to the peak start position on chromosome and the peak size (bp), respectively. ORCA and H3K9Me3 peak densities graphs were generated using composite images from IGV screenshots. Statistics were performed using Excel, GraphPad Prism and RStudio. The statistical tests and results are described in the figure legends.

Quantification and Statistical Analysis

The statistical tests and results are described in the figure legends. The Mann-Whitney test were used for statistical analysis of Fig. 1D, H, K, Fig. 3C-D, F, K, M, Fig. 5C-D, Fig. S3C, E, M, O, Q-R, and Fig. S5F. Student's t test is used for statistical analysis of Fig. 3I, Fig. 4C-E, Fig. 5H, Fig. S1C, N, Q, and Fig. S4D-E..

Reference

Arnoult, N., Van Beneden, A., and Decottignies, A. (2012). Telomere length regulates TERRA levels through increased trimethylation of telomeric H3K9 and HP1alpha. Nat Struct Mol Biol *19*, 948-956.

Feretzaki, M., and Lingner, J. (2017). A practical qPCR approach to detect TERRA, the elusive telomeric repeat-containing RNA. Methods *114*, 39-45.

Flynn, R.L., Centore, R.C., O'Sullivan, R.J., Rai, R., Tse, A., Songyang, Z., Chang, S., Karlseder, J., and Zou, L. (2011). TERRA and hnRNPA1 orchestrate an RPA-to-POT1 switch on telomeric single-stranded DNA. Nature *471*, 532-536.

Henson, J.D., Lau, L.M., Koch, S., Martin La Rotta, N., Dagg, R.A., and Reddel, R.R. (2017). The C-Circle Assay for alternative-lengthening-of-telomeres activity. Methods *114*, 74-84.

Jain, A., Liu, R., Ramani, B., Arauz, E., Ishitsuka, Y., Ragunathan, K., Park, J., Chen, J., Xiang, Y.K., and Ha, T. (2011). Probing cellular protein complexes using single-molecule pull-down. Nature *473*, 484-488.

Leigh A. Henricksen, C.B.U., Marc S. Wold (1994). Recombinanat Replication Protein A: Expression, Complex formation, and Functional Characterziation. JBC *269*, 11121-11132.

Porro, A., Feuerhahn, S., Reichenbach, P., and Lingner, J. (2010). Molecular dissection of telomeric repeat-containing RNA biogenesis unveils the presence of distinct and multiple regulatory pathways. Mol Cell Biol *30*, 4808-4817.

Scheibe, M., Arnoult, N., Kappei, D., Buchholz, F., Decottignies, A., Butter, F., and Mann, M. (2013). Quantitative interaction screen of telomeric repeat-containing RNA reveals novel TERRA regulators. Genome Res *23*, 2149-2157.

Shen, Z., Sathyan, K.M., Geng, Y., Zheng, R., Chakraborty, A., Freeman, B., Wang, F., Prasanth, K.V., and Prasanth, S.G. (2010). A WD-repeat protein stabilizes ORC binding to chromatin. Mol Cell *40*, 99-111.